Chapter 2
Self-Sensing Measurement in Piezoelectric Cantilevered Actuators for Micromanipulation and Microassembly Contexts

Ioan Alexandru Ivan, Micky Rakotondrabe, Philippe Lutz, and Nicolas Chaillet

Abstract This chapter aims to develop a self-sensing technique to measure the displacement and the force in piezoelectric microactuators dedicated to micromanipulation and microassembly contexts. In order to answer the requirements in these contexts, the developed self-sensing should perform a long duration measurement of constant signals (displacement and force) as well as a high precision. Furthermore, we propose to consider the dynamics in the displacement self-sensing measurement such that a positioning feedback is possible and therefore a high micro/nanopositioning accuracy is obtained. The experimental results validate the proposed technique and demonstrate its conveniency for micromanipulation and microassembly contexts.

Keywords Self-sensing • Force and displacement signals • Cantilevered piezoelectric actuators • Micro and nano-scale

2.1 Introduction

Piezoelectric materials are very prized to develop systems acting at the micro/nanoscale. This recognition is due to the high resolution, high bandwidth and high force density that they can offer. They can be divided into two main categories as actuators: continuous (benders, stack, tube, etc.) or discrete (stick-slip, inch-worm etc.). One of the applications of piezoelectric materials is the piezogripper (Fig. 2.1a, b) often integrated in cells (Fig. 2.1c) in order to perform micromanipulation/microassembly of small parts, such as biological objects or microstructures.

M. Rakotondrabe (✉)
FEMTO-ST Institute, UMR CNRS, 6174 - UFC, ENSMM/UTBM, rue Alain Savary 24, 25000 Besançon, France
e-mail: mrakoton@femto-st.fr

C. Clévy et al. (eds.), *Signal Measurement and Estimation Techniques for Micro and Nanotechnology*, DOI 10.1007/978-1-4419-9946-7_2,
© Springer Science+Business Media, LLC 2011

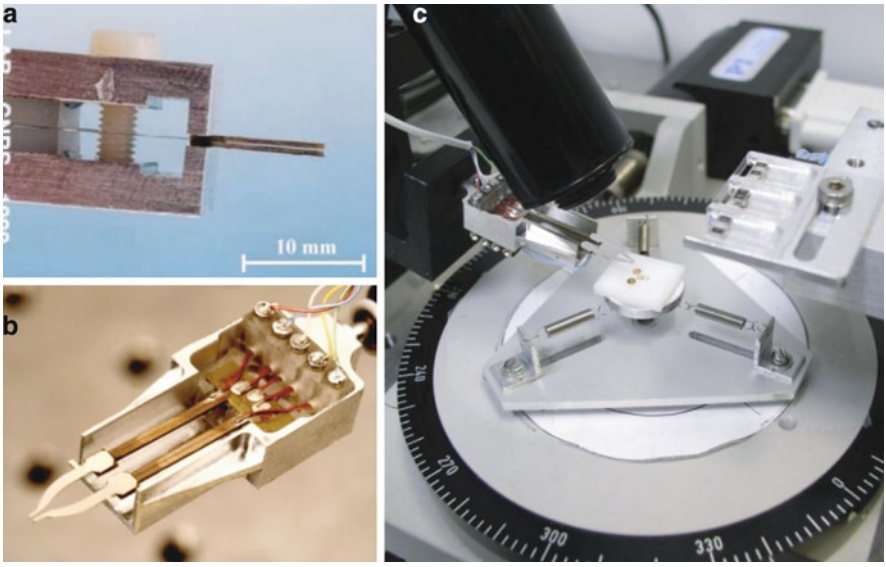


Fig. 2.1 Piezoelectric devices and systems, courtesy of AS2M Department, FEMTO-ST Institute (Besanon FR). (**a**) Double-unimorph gripper. (**b**) Duo-Bimorph gripper called MOC (Microrobot On Chip). (**c**) Working table with piezoelectric gripper

A piezogripper is made up of two piezoelectric cantilevers (piezocantilevers) (Fig. 2.2a). When the cantilevers are subjected to electric voltage, they bend and can maintain and/or position a manipulated micro-object. When properly controlled, piezogrippers can pick, transport and place micro-objects with micrometric or submicrometric positioning accuracy. While one cantilever is often controlled on position, the second one is controlled on force in order to avoid the destruction of the handled object (Fig. 2.2b). It is obvious that the successful of such control requires the measurement or estimation of the displacement and force signals. Furthermore, the availability of these signals also allow to characterize the manipulated objects if necessary.

The control and automation of piezogrippers as well as the study of the control of each elementary piezocantilever are still limited in laboratory [1, 2]. This is mainly due to the lack of embeddable and precise sensors, both for displacement and force, that can be used for packaged and feedback controlled systems. On the one hand, embeddable sensors such as strain gages are very noisy and fragile. On the other hand, very precise and large range displacement sensors (capacitive or magnetic displacement readers, optical sensors, interferometers, etc.) are bulky and expensive. Another solution can be the micromachined piezoelectric systems (Piezo-MEMS) incorporating piezoresistive or capacitive sensing elements, but these systems are not yet fully developed and available on the market. A possible solution to by-pass all these limitations is the utilization of open-loop control techniques where no sensors are required [3], but they do not account the external disturbances

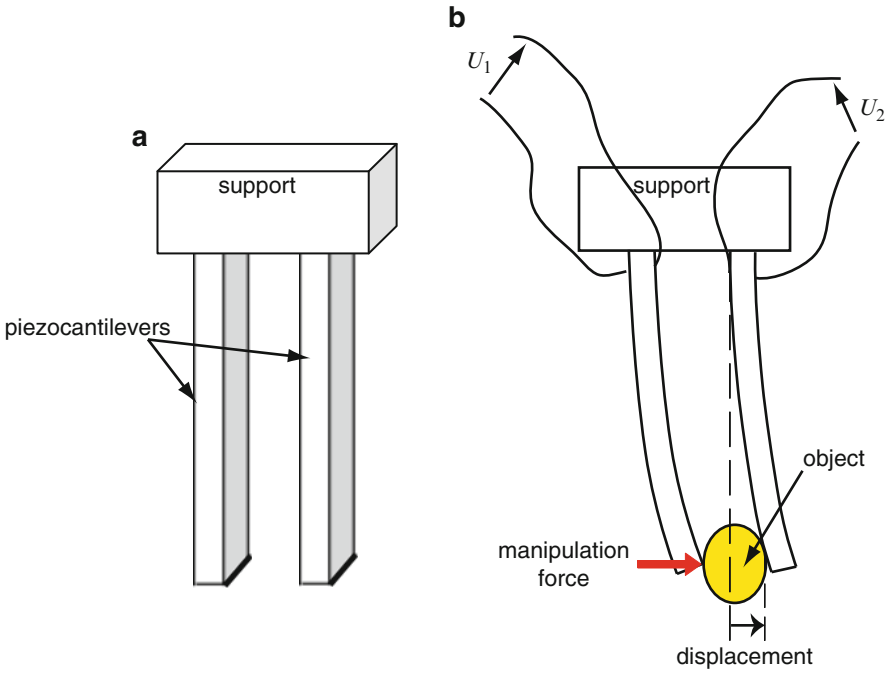


Fig. 2.2 (**a**) Principle of a piezogripper. (**b**) Manipulation of a micro-object

(such as thermal variation) as well as the internal uncertainties of the actuators models making therefore the loss of the accuracy. To sum up, it appears that existing methods in piezogrippers control do not answer the requirement of high performances and the packageability and that newer approach should be proposed for that.

In this chapter, we propose to apply the self-sensing approach to measure the signals in piezocantilevers of a piezogripper. Self-sensing has the advantages to be directly packaged and to offer a feedback control possibility if well designed. It is, therefore, suitable for the developement of embedded and high performances piezogrippers dedicated to micromanipulation and microassembly cells.

Self-sensing consists of using at the same time an actuator as also a sensor. This is particularly achievable for piezoelectric actuators thanks to the direct and converse piezoelectric effects, subjected that convenient electric circuit and observer are used. This simple and cost-effective up-grade solution for existing piezoelectric grippers is based on current integration, that allows displacement and/or force measurement. Charge measurement is often rejected on false idea that PZT is a very bad isolating material. In fact, not the leaking resistivity, which is high enough to preserve charges for hundreds of seconds, but ferroelectric material non-linearities (hysteresis, creep) as well as temperature influence put challenge on charge-based self-sensing. Existing literatures in self-sensing methods do not account both hysteresis and creep compensations. In addition, they are only intended

for vibrations or short-term duration; hence, they are not convenient for quasi-static requirements such as in micromanipulation/microassembly.

The idea of self-sensing in piezoelectric cantilever has been started by the work of Dosch et al. [4]. While it is not a new concept on vibration damping and related control [5, 6], more recently, it has shown its feasibility for piezoelectric tubes of atomic force microscopy [7, 8]. Despite the efficiency of self-sensing techniques for measurement in dynamics, they have not yet been adapted for long-term measurement (more than hundreds of seconds) of displacement and/or force in cantilevered actuators, as required by micromanipulation and microassembly applications. In this chapter, we propose therefore electric schemes followed by convenient observers in order to be able to measure constant values of displacement and the force in piezocantilevers. We afterwards extend the proposed scheme to include both the dynamic and static apsects for the displacement measurement such that a feedback control to enhance the performances is possible. The presented results are extension of our three previous works [9–11]. The nonlinearities, mainly the hysteresis and the creep, which typify piezoelectric materials are compensated.

The chapter is organized as follows. In Sect. 2.2, we provide some fundamentals on piezoelectricity. In Sect. 2.3, we detail the self-sensing for constant long-term measurement of displacement. Section 2.4 is an extension of the displacement static self-sensing in order to include the force. In Sect. 2.5, we propose to consider the dynamic self-sensing for the displacement. Finally, we give some conclusions in Sect. 2.6.

2.2 Fundamentals of Piezoelectric Actuators and Self-Sensing

2.2.1 Piezoelectric Cantilevered Actuators

In piezogrippers, according to the geometry of the piezocantilevered actuators, displacement scale ranges from micrometer to millimeter, and usual blocking force from 100 μN to 100 mN. Micro-position accuracy can go down to a couple nanometers and response time is in the order of milliseconds. In the sequel, the terms *piezoelectric cantilever* and *piezocantilever* are alternately employed.

Piezocantilevers are usually made of piezoelectric PZT ceramics ($Pb[Zr_x Ti_{1-x}]O_3$) and amorphous (mettalic) materials. Polymers such as PVDF (polyvinylidene fluoride) are rarely employed. Unimorph cantilevers are made of a single layer of piezoelectric material deposited or stuck on an amorphous base material (cross-section shown in Fig. 2.3a). When an external electric field is applied, the piezoelectric layer tends to contract/expand making the whole structure to bend (Fig. 2.4) accordingly to well-stated constitutive equations [12] and depicted briefly in Sect. 2.3. Bimorph actuators (Fig. 2.3b, c) are made up of two piezoelectric layers that are to be driven in an opposite manner (depending on polarization direction). Main advantage with respect to unimorphs is the increase of displacement range, blocking force and a better temperature effects rejection.

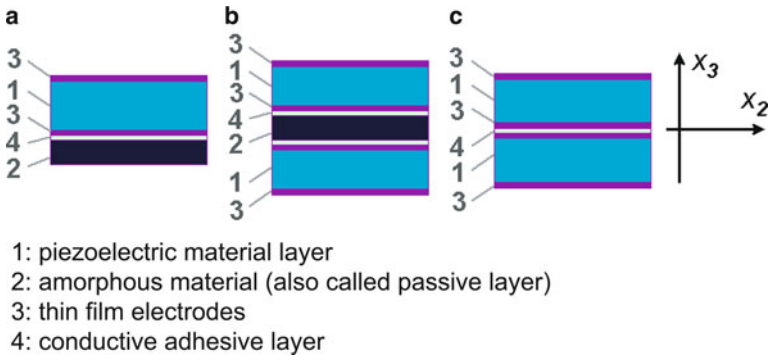


Fig. 2.3 Cross-section of different piezoelectric bender structures: (**a**) unimorph, (**b**) three-layer bimorph, (**c**) two-layer bimorph

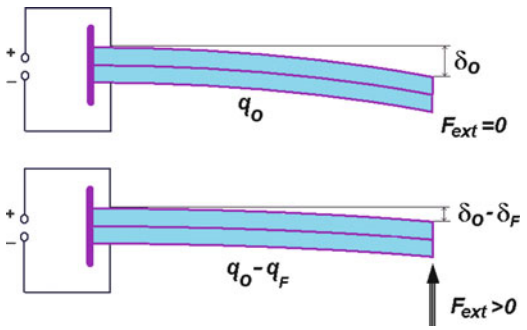


Fig. 2.4 Electric charge in a piezoelectric cantilever bending under external voltage

With the advent of multiple screen-printing and sol-gel techniques, multi-layer piezocantilevers applications are also raising [12, 13].

Given the continuous interest in piezoelectric actuators over the past decades, the literature is rich in studying and modeling these devices behaviour, static, and dynamic nonlinearities as well as their limits [14–17] for providing closed or open loop control solutions.

2.2.2 Self-Sensing: Methods, Challenges, and Applications

Self-Sensing allows actuating a piezoelectric device while sensing its displacement (strain) and/or applied force (stress). The intrinsic technique may be further used in a closed-loop system without needing external sensors.

The first use of "self-sensing" term dates back to 1992 when Dosch et al. [4] while his work consisted in successfully damping the vibration of a piezoelectric beam without using the aid of external sensors. Voltage drop provided from a capacitive bridge was processed in an analog circuit, amplified and returned back to the piezoelectric element. Sooner, several independent applications began to emerge

for beam vibration control or stack micropositioning piezo devices. Several years later T. Taigami et al. [18] applied the method for force self-sensing and control of a large size bimorph actuator, using a half-bridge circuit, a voltage follower and PC-based data acquisition system. The authors experimentally verified that the stiffness of the grasping object does not affect the measurement; however, electronic schematic limited applied voltage range and nonlinearities (hysteresis and creep) were not compensated.

Creep compensation by shaping the applied step signal with a logarithmic function allowed a reduction of open loop control error by a factor of 5–10 [19]. Issues related to compensation of hysteresis and creep with inverse systems came also into discussion [20]. In [21], hysteresis and creep models were inverted using Newton iterative procedure, reported displacement open loop control error being 2% (not specified if on full actuator range). In [22], adaptive identification based on an unscented Kalman filter was proposed to make dynamic prediction of a first order nonlinear hysteresis behaviour for a piezo stack actuator. Without entering into details especially on creep detection, maximum reported percentage error for hysteresis and creep was 3.2 and 1.2% respectively.

Concerning self-sensing, an integrator-based circuit was introduced [23] to sense and control a piezo stack displacement. This basic principle of circuit is closed to that of proposed in our previous work [9], showing advantages over bridge-based circuit. The paper [23] is focused on a compounding control of displacement combining a PID feedback control and a feedforward control of hysteretic behavior. Self-sensing force control for piezo stack was introduced in [24, 25]. The voltage drop on a RC shunt circuit is used to calculate the charges. A hyperbola-shaped operator was used to model separately ascending and descending branches of the hysteresis. Force is controlled classically with a PID feedback under different loading conditions. In paper [26], a generalized Maxwell-slip hysteresis operator was used. Static displacement error is reported to 2–4% while static force error is 2–6%.

The issues of these papers focus on short-term (less than 1 s) force self-sensing control or vibration damping applications. For instance in [5], a modified bridge circuit with adaptable gain was intended for vibration control under structural deformation, in [6] self-sensing actuators ameliorated positioning and vibration in hard-disk drives, in [27] self-sensing microdispensing system demonstrated better positioning performance than with external sensors.

Some sensorless methods neighbored to self-sensing concept consist in shaping several electrodes on actuator and dedicating them separately for actuating or sensing [28]. In this way, nonlinear effects are avoided and signals well separated. However, a fraction of actuating capability is lost. Recently, a SPM piezo-tube scanner with a new electrode pattern allowed self-measurement of nanometer resolution with improved transfer function [7, 8].

Summarizing, self-sensing first advantage is that system will be more flexible in terms of space occupation, allowing better miniaturization and dexterity in terms of DoF (degrees of freedom). Also, actuator's dynamics will no longer be affected by mechanically attached sensors (e.g. strain gages). The number of connecting cables will be reduced. The system will be more cost-effective.

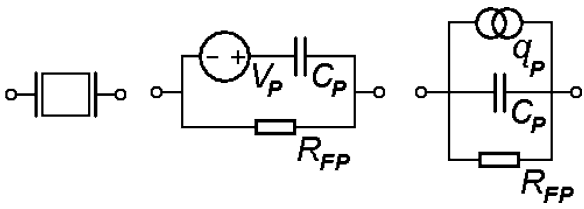


Fig. 2.5 Symbol and equivalent electrical schematics of piezo actuators

Disadvantages consist in adding a supplementary electronic circuit, but of reduced complexity. On the other hand, provided measurement is not fully-static. Electronic circuit is based on a capacitive bridge (or divider) or a current integrator. Specific applications with dedicated electrodes for sensing may measure directly strain-induced voltage. Attention has to be paid for preserving the charge as long as possible. Non-linearities such as hysteresis and creep due to ferroelectric domain relaxation put the most challenge on self-sensing technique, limiting its accuracy, especially in force sensing. Identifying these nonlinear effects requires an extra procedure. Finally, there are working temperature constraints that should be taken into account to prevent loss of accuracy.

Very few publications deal with self-sensing techniques intended for automated or tele-operated micromanipulation/microassembly cells. For these systems, the required periods of time for preserving the static values are between dozens to several hundreds of seconds. A quasi-static method for deriving displacement and force from actuated uni- and bi-morph cantilevers is therefore proposed in the sequel. The nonlinearities (hysteresis and creep) are especially taken into account.

2.2.3 Electronic Circuit and Experimental Setup

In Fig. 2.5, static equivalent schematic is shown. C_P is the piezo element capacitance, R_FP is the PZT leaking resistance (in the $G\Omega$ range) and V_P and q_P are the piezoelectrically generated voltage or charge, respectively.

The electronic schematic as in Fig. 2.6 integrates the current across the actuator. It provides the main signal for the self-sensing observer. An optional fixed value C_R capacitor in anti-parallel with C_P improves signal range by keeping the same sensitivity.

Output voltage of the circuit is:

$$V_\mathrm{out} = -\frac{1}{C}\int_0^T i(t)\mathrm{d}t = -\frac{1}{C}Q. \tag{2.1}$$

Where the charge Q varies with the applied voltage and is proportional with the capacitance difference $(C_\mathrm{P} - C_\mathrm{R})$. In reality, as will be seen, nonlinear ferroelectric

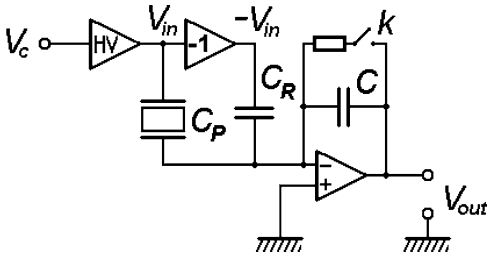


Fig. 2.6 Electronic circuit schematic of charge amplifier [9]

effects and slow charge leaks in the piezoelectric material will require several compensation terms. Supplementary practical details of the circuit design and how to improve its parameters are presented in [9].

The experimental setup is depicted in Fig. 2.7a, b. Several rectangular actuators (made of PZT bonded on a *Cu* or *Ni* substrate) were tested, of length between 10 and 15 mm, width between 1 and 2 mm, and total thickness of 0.27–0.45 mm. The FemtoTools force sensor and the optical displacement reader type Keyence LC-2420 were used for only intermediate tests. Also a SIOS SP-120 miniature plane-mirror interferometer was employed if higher resolution was necessary. The high voltage (HV) amplifier allowed supplying the actuator with a voltage up to 150 V. The DSpace DS1103 real-time controller board served to implement under Matlab Simulink the required observers, as will be detailed in the next chapters.

2.3 Static Displacement Self-Sensing

2.3.1 Charge Calculation

The developed self-sensing systems can be divided into three main parts, as in Fig. 2.8. In the figure, V_{in} is the applied input voltage, δ is the deflection of the cantilever while $\hat{\delta}_{\text{s}}$ is the estimate from the self-sensing. Q is the charge appearing on the surfaces of the electrodes and V_{out} is the voltage from the electronic circuit. The piezoelectric actuators and the charge amplifier (current integrator) were previously discussed. Acquired V_{out} signal is processed to provide detected displacement. For this purpose a data processing system should implement an observer (estimator).

In the absence of external force, we have a theoretically linear relation between displacement and applied voltage [29]:

$$\delta = -\frac{3d_{31}}{1+\frac{d_{31}^2}{4s_{11}^E\varepsilon_{33}^S}}\frac{L^2}{h^2}V_{\text{in}}, \tag{2.2}$$

where s_{11}^E is the compliance coefficient along the beam, ε_{33}^S and d_{31} are dielectric and piezoelectric material coefficients.

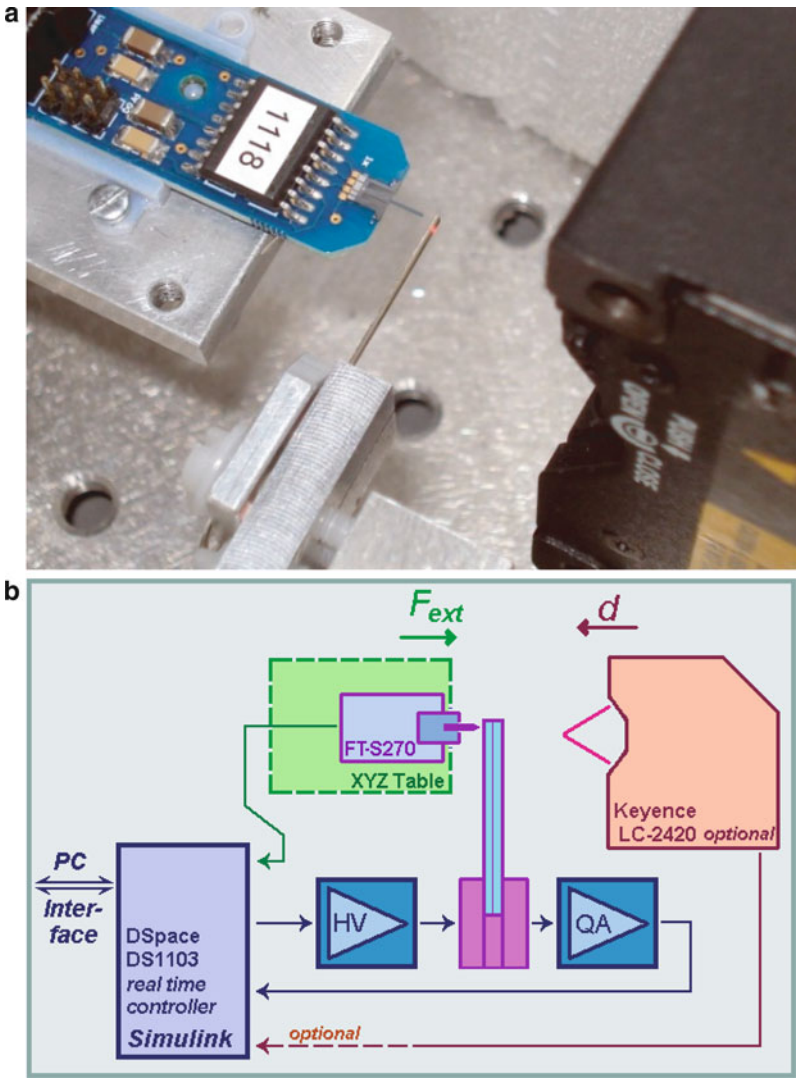


Fig. 2.7 (**a**) Photo of experimental set-up. A force sensor is on the *left*, the actuator is in the *middle* and an optical displacement reader is located in the *right side* of the image. (**b**) Schematic block diagram used for experiments, consisting of the piezoactuator, force and displacement sensors, high voltage amplifier (HV), charge amplifier (QA) and real-time controller. Directions for positive force and displacement are figured

Using the relation between the applied voltage and the capacitance for bimorph piezoelectric cantilever beam

$$Q = \frac{4wL\varepsilon_{33}^{S}}{h} V_{\text{in}} \tag{2.3}$$

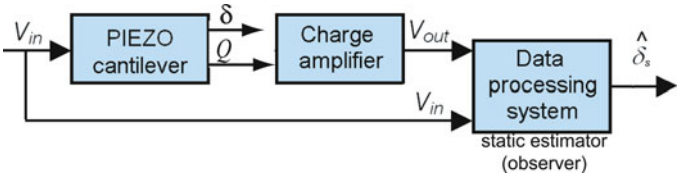


Fig. 2.8 Principle of the static displacement self-sensing

charge directly results and, as stated previously, is quasi-proportional to free displacement δ:

$$Q = \frac{4whd\varepsilon_{33}^S}{3d_{31}L}\left(1 + \frac{d_{31}^2}{4s_{11}^E\varepsilon_{33}^S}\right)\delta = \alpha\delta, \tag{2.4}$$

where α is denoted as an actuator charge-displacement coefficient.

In the sequel, this charge will be converted into a measurable voltage V_{out} from which the deflection δ will be estimated as described in Fig. 2.8.

If we consider the circuit from Fig. 2.6, in the absence of the external force ($F_{\text{ext}} = 0$), charge converted by the operational amplifier is:

$$Q = -C_{\text{R}}V_{\text{in}} + \alpha\delta. \tag{2.5}$$

Finally, we noticed a nonlinearity very similar to the dielectric absorption effect in capacitors. This effect is also common in piezoelectric materials, in consequence we proposed adding a third term Q_{DA} which is an internal amount of charge depending on ε_{33} variation:

$$Q = -C_{\text{R}}V_{\text{in}} + (\alpha\delta + Q_{\text{DA}}). \tag{2.6}$$

2.3.2 Estimated Displacement Formula

The output voltage V_{out} of the free cantilever beam also depends on the influence of the op-amp non-zero bias current i_{BIAS} and of the piezoactuator finite leaking resistance R_{FP}:

$$V_{\text{out}} = \frac{C_{\text{R}}}{C}V_{\text{in}} - \frac{\alpha\delta + Q_{\text{DA}}}{C} - \frac{1}{C}\int\frac{V_{\text{in}}(t)}{R_{\text{FP}}}\text{d}t - \frac{1}{C}\int i_{\text{BIAS}}(t)\text{d}t. \tag{2.7}$$

The estimated displacement $\hat{\delta}_s$, may be computed as follows:

$$\hat{\delta}_s = -\frac{C}{\alpha}V_{\text{out}} - \frac{Q_{\text{DA}}(V_{\text{in}},t)}{\alpha} + \frac{C_{\text{R}}}{\alpha}V_{\text{in}} - \frac{1}{R_{\text{FP}}\alpha}\int V_{\text{in}}(t)\text{d}t - \frac{1}{\alpha}\int i_{\text{BIAS}}(t)\text{d}t. \tag{2.8}$$

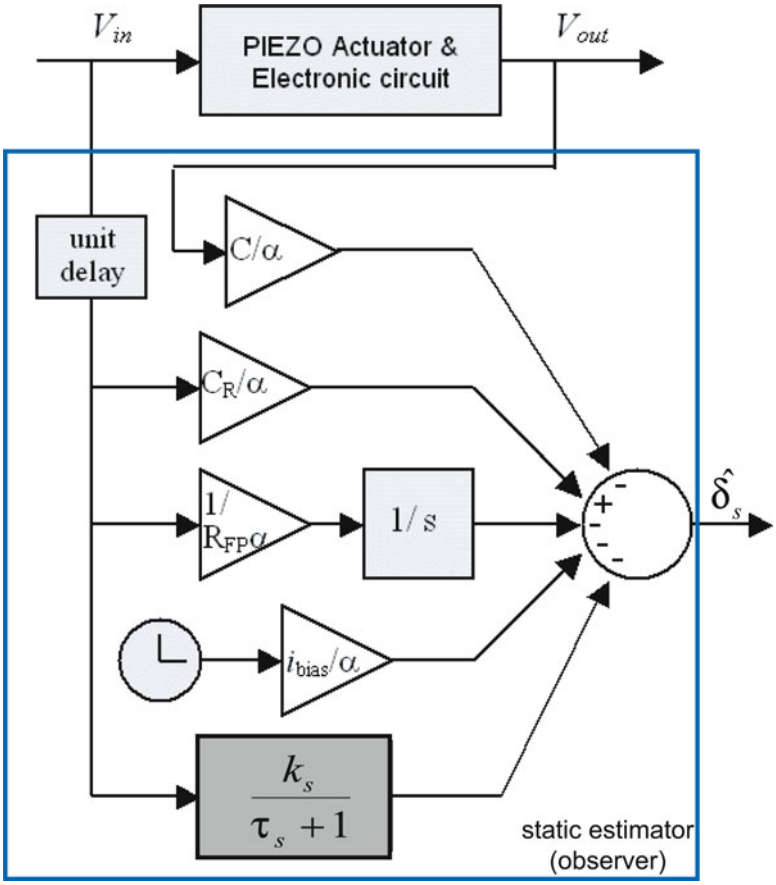


Fig. 2.9 Block-scheme (in Simulink) of the observer of the static displacement self-sensing. Reprinted with permission, Copyright 2009 American Institute of Physics [9]

Regarding the dielectric absorption term, we will consider a simple relaxation effect described by a simple first-order transfer function:

$$Q^*_{\mathrm{DA}}(V_{\mathrm{in}}, s) = \frac{Q_{\mathrm{DA}}(V_{\mathrm{in}}, s)}{\alpha} = \frac{k_{\mathrm{s}}}{\tau s + 1} V_{\mathrm{in}}, \tag{2.9}$$

where k_{s} is a static gain and τ a time constant.

Figure 2.9 presents the final observer bloc-scheme. Some parameters of the expression (8) are known while others require identification. Their calculation will be presented in the next section.

2.3.3 Parameters Identification

The identification of unknown parameters (α, i_{BIAS}, R_{FP}, Q_{DA}) can be performed under a manual or semi-automatic procedure. External sensors are required for this one-time only procedure. The displacement δ is provided by the displacement sensor (optical or interferometer). The following steps describe the identification procedure.

2.3.3.1 Bias Current i_{BIAS} Identification

It should be noted that bias current varies exponentially with the temperature, so proper care must be insured with the electronic circuit. i_{BIAS} currents for a good operational amplifier are below $1pA$. Under $F_{\text{ext}} = 0$, $V_{\text{in}} = 0$, $V_{\text{out}} \cong 0$ and zero temperature change, there is no electric current through the piezoelectric material. The V_{out} rate of change is measured for several dozens of seconds, deriving i_{BIAS}.

2.3.3.2 Leaking Resistance R_{FP} Identification

Under $F_{\text{ext}} = 0$, a constant voltage ($V_{\text{in}} \neq 0$) is applied to the actuator. After several hundred seconds the creep influence becomes constant, and the output voltage V_{out} shifts with a constant slope, depending only on i_{BIAS} (identified before) and R_{FP} (to be identified). The identification can be repeated for different V_{in} values whose results are afterwards averaged. Each point on Fig. 2.10 was recorded after a 1,000–2,000 s delay, to eliminate residual creep influence. Linear regression was applied. Quality piezo cantilevers will exhibit R_{FP} values superior to 1,010 Ω. For our actuator we identified $R_{\text{FP}} = 0.435\,\text{T}\Omega$.

2.3.3.3 Displacement Coefficient α Identification

A step signal is applied on the free actuator. To avoid oscillatory of the actuator, the step signal is shaped with ramp of around 20 V/s (Fig. 2.11). Measured values of δ and V_{out} immediately after the step signal V_{in} will serve to compute α:

$$\alpha = (-CV_{\text{out}} + C_{\text{R}}V_{\text{in}})/\delta. \tag{2.10}$$

An alternate method for deriving α is to apply one or several sinusoidal signals as in Fig. 2.12 and use amplitude values in (2.10), i.e. use magnitude at low frequency.

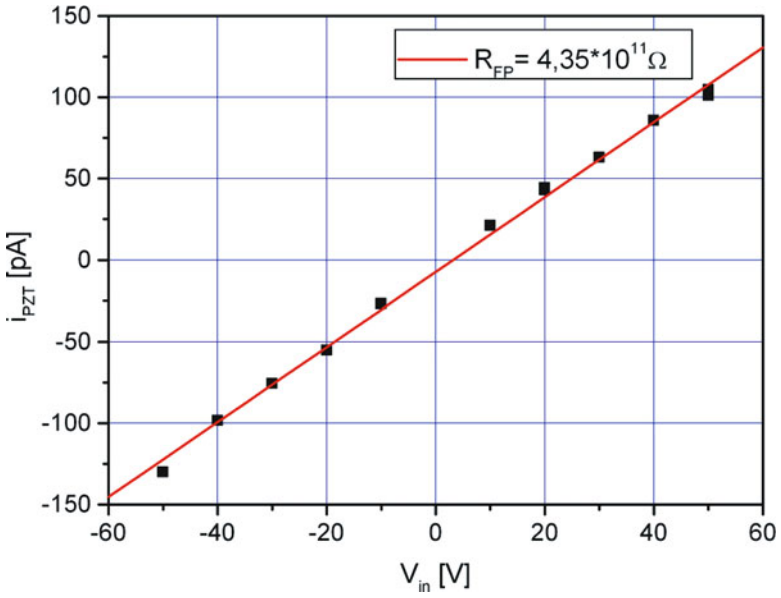


Fig. 2.10 Leakage current of PZT actuator measured under constant DC voltage values. Calculated insulation resistance is 0.435 TΩ. Reprinted with permission, Copyright 2009 American Institute of Physics [9]

2.3.3.4 Identification of Dielectric Absorption Transfer Function

The last part to be identified in displacement formula (2.8) is the dielectric absorption $Q_{\mathrm{DA}}(V_{\mathrm{in}},t)$ of the piezoelectric material. We have:

$$\Delta\hat{\delta}_s(s) = Q^*_{\mathrm{DA}}(s)V_{\mathrm{in}}(s), \tag{2.11}$$

where $\Delta\hat{\delta}_s = \hat{\delta}_s - \delta$ is the difference between estimated (using already identified parameters) and measured tip displacement.

Identification of k_{s} and τ is performed on a step response, allowing the calculation of the static gain and time constant easily (Fig. 2.13).

2.3.4 Displacement Self-Sensing Results

In Fig. 2.14, an input signal V_{in} was applied in several steps between $+20$ and -25 V, under null external force. Data was recorded for 1,020 s – sufficient for most micromanipulation and microassembly applications involving piezoelectric actuators. A very good agreement is found: measured and detected displacement curves almost superpose.

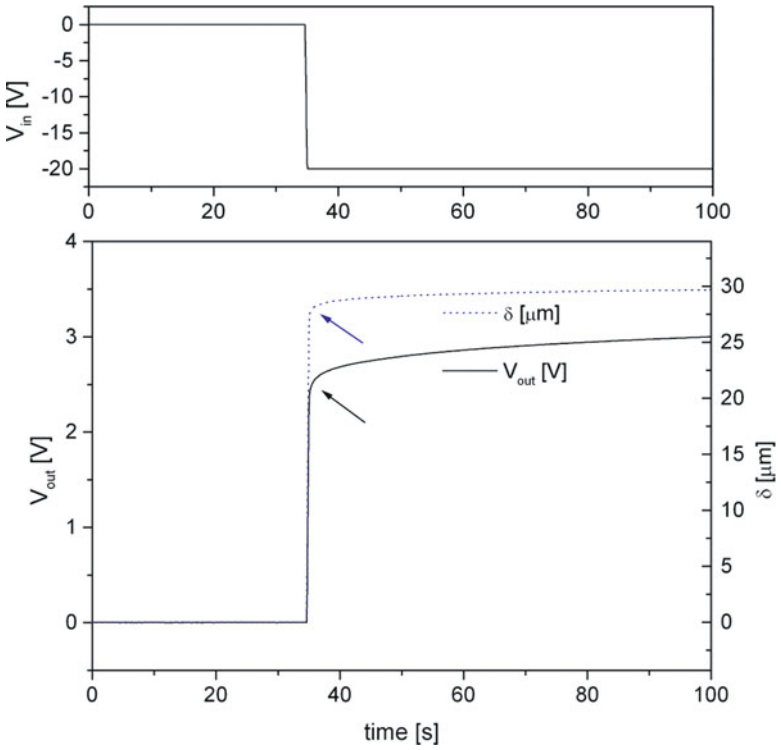


Fig. 2.11 Identification of α coefficient from -20 V step input voltage. Reprinted with permission, Copyright 2009 American Institute of Physics [9]

A comparative representation of displacement errors is made as follows. Three graphs are traced (Figs. 2.15–2.17), from uncompensated to fully compensated with respect to leaking resistance and dielectric absorption. Measurement with Keyence optical displacement reader provided a poorer linearity than self-sensing signal, making impossible accurate error evaluation, SIOS interferometer was eventually employed. Our constraint on the utilized interferometer is that data is only available offline. Vertical error lines in the figures can be neglected and are due to the linear interpolation and sampling period mismatch between the two data sets (acquired at sampling rates of 10 and 16.11 Hz). As seen in the Fig. 2.15, peak-to-peak error of uncompensated signal is 2.75 μm. Compensation of R_{FP} leaking resistance allowed a reduction of maximum error to 1.05 μm (Fig. 2.16). Adding the compensation of dielectric absorption (Fig. 2.17) provided a 0.38 μm (0.55%) peak-to-peak error.

Unaveraged measured self-sensing signal noise in displacement (Fig. 2.18) is of only 1.6 nm (RMS), being ten times less noisy than that of filtered Keyence LC-2420 sensor (16.7 nm rms noise on 4096 averaged samples). However, as expected, SIOS SP 120 interferometer showed best results: 0.5 nm rms noise.

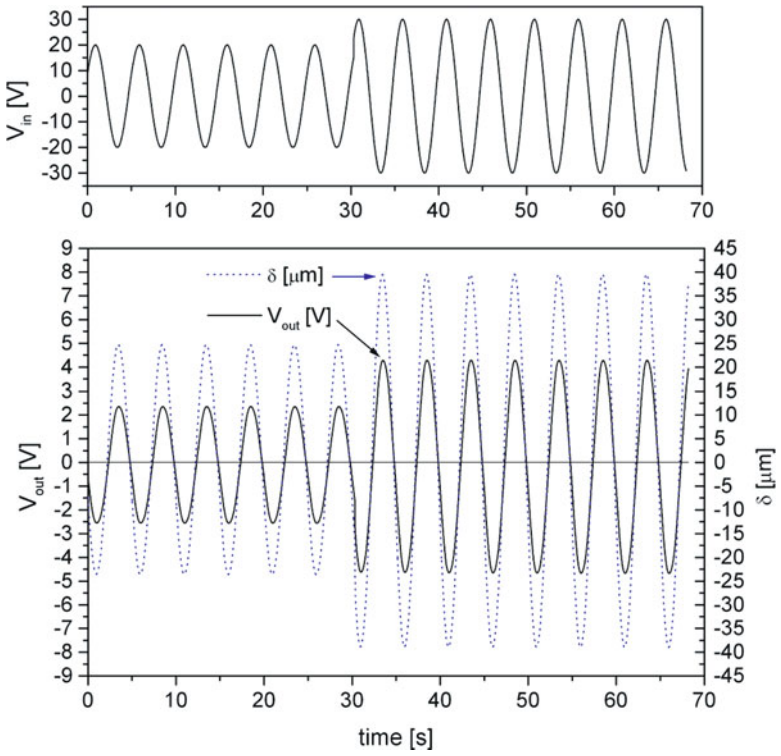


Fig. 2.12 Identification of α coefficient from sinusoidal signals. Reprinted with permission, Copyright 2009 American Institute of Physics [9]

2.4 Static Displacement and Force Self-Sensing

2.4.1 Force-Displacement Self-Sensing Detection

A self-sensing system for displacement and force detection can be divided into three main parts, as in Fig. 2.19. Piezoelectric actuator is submitted to a known input voltage V_{in} and to an unknown external force F_{ext}. Resulted charge Q is converted by an electronic amplifier to a measurable voltage V_{out}. Acquired signal is processed to provide detected displacement and/or force.

Observer algorithm runs on a PC or is deployed into a real-time processor or microcontroller. External signals can be provided to improve self-sensing accuracy, for instance temperature variation compensation. As the charge cannot be kept indefinitely, external resetting before each measurement could offset large parts of the error. Externally provided close-contact information could also help observers in ameliorating force sensing.

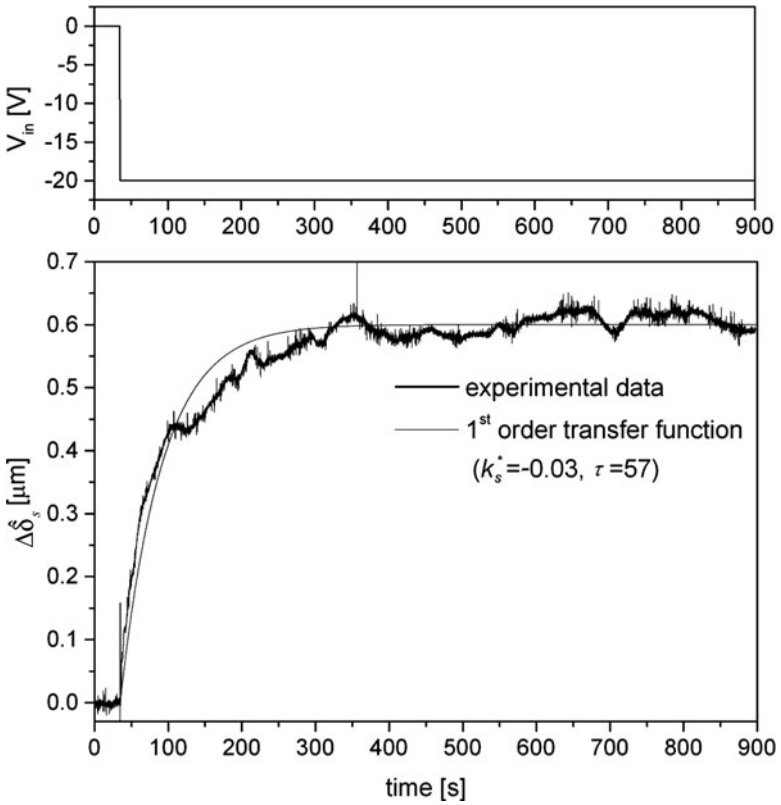


Fig. 2.13 Identification of dielectric absorption $Q^*_{\mathrm{DA}}(s)$ transfer function. Reprinted with permission, Copyright 2009 American Institute of Physics [9]

2.4.2 Piezoelectic Bimorphs: Theoretical Approach

The force equilibrium of a cantilever can be simplified as:

$$\mathbf{F}_{\mathrm{ext}} + \mathbf{F}_{\mathrm{el}} + \mathbf{F}_{\mathrm{piezo}} = 0, \tag{2.12}$$

where F_{ext} is the external force (to evaluate), $F_{\mathrm{el}} \cong k_{\mathrm{beam}}\delta$ is the elastic bending force (proportional to the beam flexure δ) and F_{piezo} is the reverse piezoelectric effect generated force.

When an external electrical field E_3 is applied along z-axis (poling direction), stress along x-axis T_1 and electrical displacement along z-axis D_3 are:

$$T_1 = c_{11}S_1 - e_{31}E_3, \tag{2.13}$$

$$D_3 = \varepsilon^S_{33}E_3 + e_{31}S_1, \tag{2.14}$$

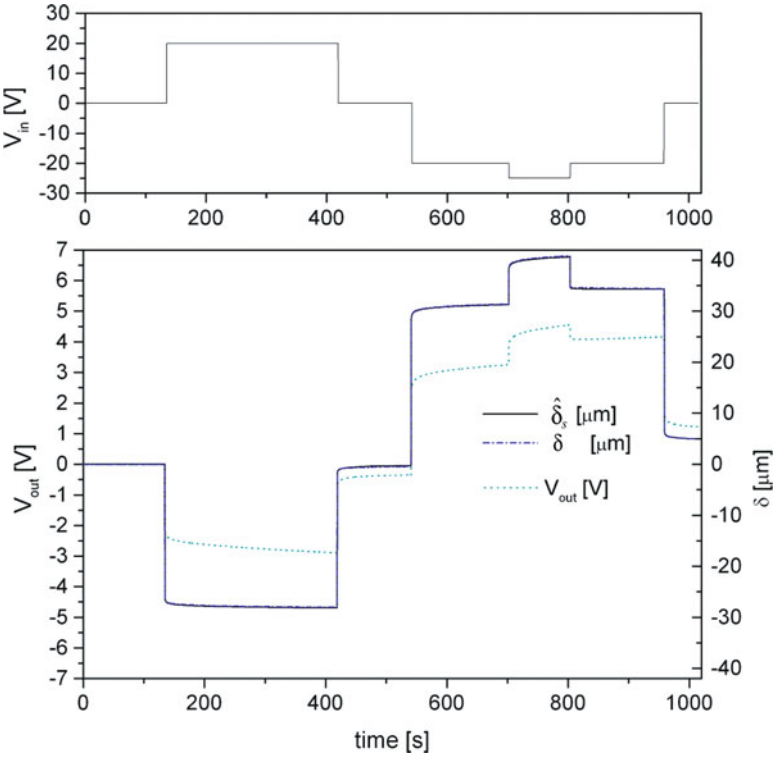


Fig. 2.14 Measured and detected displacement for an arbitrary V_{in} input signal ($F_{\text{ext}} = 0$). Reprinted with permission. Copyright 2009 American Institute of Physics [9]

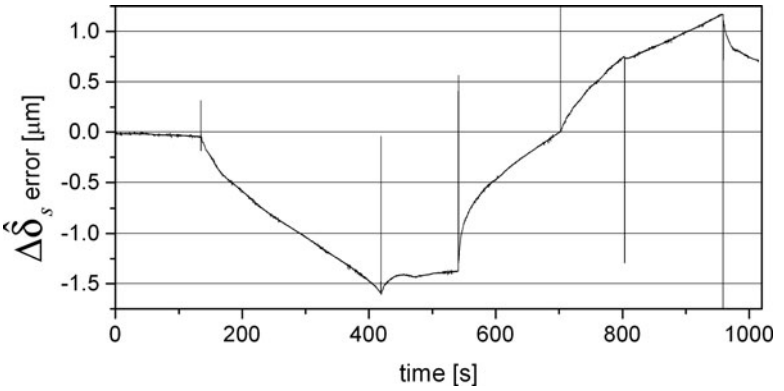


Fig. 2.15 Error curve of detected displacement with no leaking resistance R_{FP} and dielectric absorption Q_{DA} compensation. Reprinted with permission, Copyright 2009 American Institute of Physics [9]

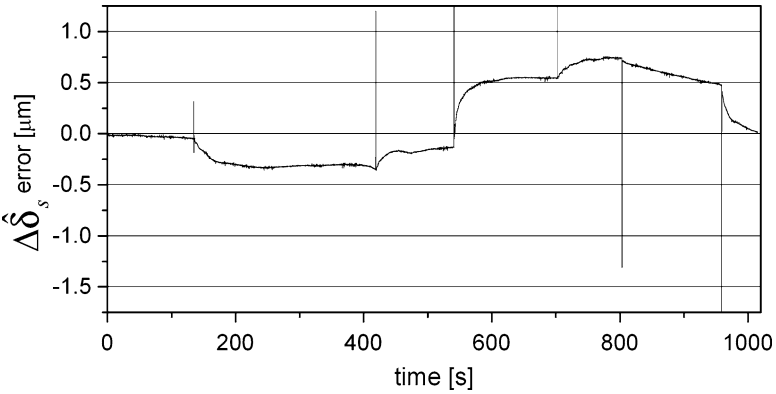


Fig. 2.16 Error curve of detected displacement with only leaking resistance R_{FP} compensation. Reprinted with permission, Copyright 2009 American Institute of Physics [9]

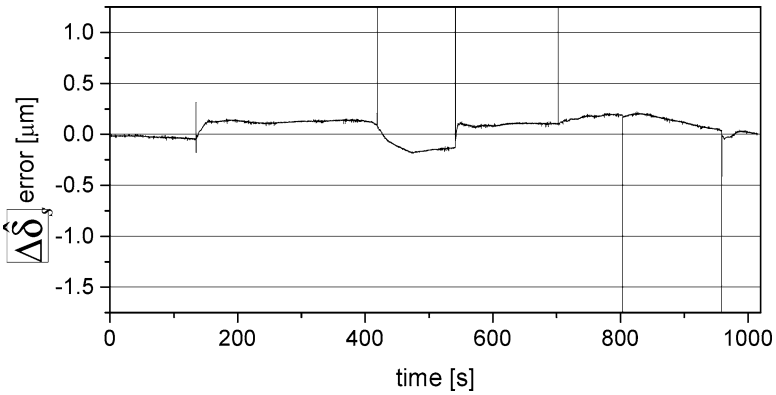


Fig. 2.17 Error curve of detected displacement with compensation of leaking resistance R_{FP} and dielectric absorption Q_{DA}. Reprinted with permission, Copyright 2009 American Institute of Physics [9]

or

$$D_3 = \varepsilon_{33}^T E_3 + d_{31} T_1, \tag{2.15}$$

where c_{11}, d_{31}, e_{31} and ε_{33} are stiffness, strain-charge and stress-charge piezoelectric coefficients and dielectric material constants. Variable S_1 denotes strain along x-axis.

We will consider a cantilevered bimorph beam of length L, width w and thickness $\pm h/2$ (Figs. 2.3 and 2.20) submitted to an external voltage V_{in}. For a small portion in circular flexure the strain at a distance x_3 from neutral fiber is:

$$S_1 = \frac{\mathrm{d}S_1 - \mathrm{d}S_0}{\mathrm{d}S_0} = \frac{(R + x_3 - R)\mathrm{d}\alpha}{R\mathrm{d}\alpha} = \frac{x_3}{R}. \tag{2.16}$$

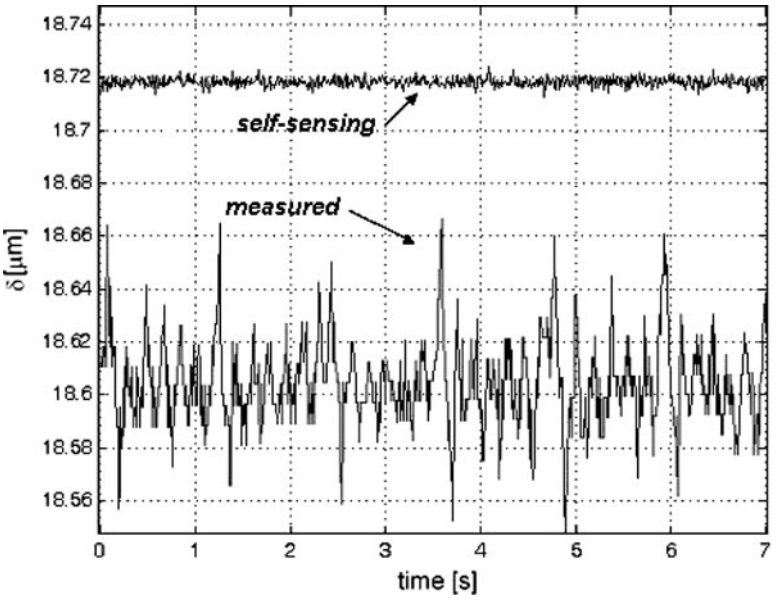


Fig. 2.18 Zoomed measured (Keyence LC2420) and detected displacement for noise evaluation. Reprinted with permission, Copyright 2009 American Institute of Physics [9]

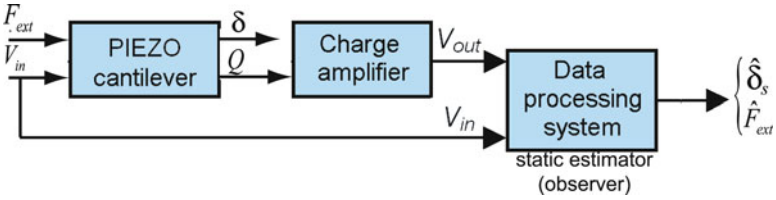


Fig. 2.19 Principle of the static displacement and force self-sensing

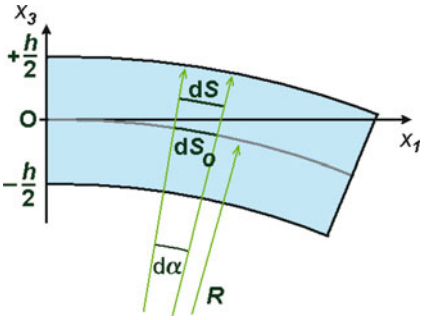


Fig. 2.20 A piezocantilever in its bending mode

Curvature radius is:

$$R = YI/M = \frac{Ywh^3}{12F_{\text{ext}}(L-x_1)}, \tag{2.17}$$

where Y is elasticity modulus, I is the x_1-axis moment of inertia and M is the bending moment of F_{ext} force.

Starting from Gauss theorem ($\nabla D = 0$) and using (2.14) and (2.16) it can be demonstrated that the bimorph electric field formula is:

$$E(x_3) = \frac{e_{31}h}{4\varepsilon_{33}R} - \frac{e_{31}x_3}{\varepsilon_{33}R} - \frac{2V_{\text{in}}}{h}. \tag{2.18}$$

Electric displacement on both sides is:

$$D_3(\pm h/2) = \pm\frac{e_{31}h}{4R} \mp \frac{2\varepsilon_{33}V_{\text{in}}}{h}. \tag{2.19}$$

Superficial charge density σ is:

$$\sigma = -D_3(+h/2) + D_3(-h/2) = -\frac{e_{31}h}{2R} + \frac{4\varepsilon_{33}V_{\text{in}}}{h}. \tag{2.20}$$

Charge due to applied voltage and external force is:

$$Q = \int\int_A \sigma \mathrm{d}x_1\mathrm{d}x_2 = \int_0^L\int_0^w \left[-e_{31}\frac{h}{2}\frac{12F_{\text{ext}}}{Ywh^3}(L-x_1) + \frac{4\varepsilon_{33}V_{\text{in}}}{h}\right]\mathrm{d}x_2\mathrm{d}x_1. \tag{2.21}$$

which derives:

$$Q = -3e_{31}s_{11}\frac{L^2}{h^2}F_{\text{ext}} + \frac{4Lw\varepsilon_{33}V_{\text{in}}}{h} = \beta F_{\text{ext}} + C_{\text{P}}V_{\text{in}}, \tag{2.22}$$

where β is the force sensitivity coefficient and C_{P} is the actuator capacitance.

Displacement of the beam submitted to external voltage and force is derived from reference [29]:

$$\delta = \frac{4s_{11}^E}{1+\frac{d_{31}^2}{4s_{11}^E\varepsilon_{33}^S}}\frac{L^3}{wh^3}F_{\text{ext}} - \frac{3d_{31}}{1+\frac{d_{31}^2}{4s_{11}^E\varepsilon_{33}^S}}\frac{L^2}{h^2}V_{\text{in}}. \tag{2.23}$$

In Sect. 2.4.4, the exact formulae for displacement and force estimation will be introduced.

2.4.3 Experimental Setup

The setup schematic overview is depicted in Fig. 2.7. Reference force is measured with a FT-S270 micromachined capacitive sensor (from *FEMTO-tools* company)

mounted on a XYZ micro-translation table for close-contact adjustment. The displacement is measured by a Keyence LC-2420 optical head. Both sensors are employed as reference in identification and error evaluation tests, their presence is of course finally not necessary when the self-sensing method is used.

Recall the equation of the output voltage already presented in (2.1):

$$V_{\text{out}} = -\frac{1}{C}\int_0^T i(t)\mathrm{d}t = -\frac{1}{C}Q, \tag{2.24}$$

where, if we ignore all non-linear piezoelectric effects, charge is proportional to applied voltage V_{in} and external force F_{ext} like in (2.22):

$$Q = (C_{\text{P}} - C_{\text{R}})V_{\text{in}} + \beta F_{\text{ext}}. \tag{2.25}$$

2.4.4 Detected Displacement and Force Formulae

Formulae (2.24)–(2.25) require further compensation against op-amp bias current i_{BIAS} and piezoelectric actuator leaking resistance especially when working in quasi-static (more than a couple seconds of integration time). When we are in force detection mode, the expression (2.24) becomes:

$$V_{\text{out}} = \frac{C_{\text{R}} - C_{\text{P}}}{C}V_{\text{in}} - \frac{\beta F_{\text{ext}}}{C} - \frac{1}{C}\int \frac{V_{\text{in}}(t)}{R_{\text{FP}}}\mathrm{d}t - \frac{1}{C}\int i_{\text{BIAS}}(t)\mathrm{d}t. \tag{2.26}$$

Hence, estimated external force is:

$$\hat{F}_{\text{ext}} = -\frac{C}{\beta}V_{\text{out}} + \frac{C_{\text{R}} - C_{\text{P}}}{\beta}V_{\text{in}} - \frac{1}{R_{\text{FP}}\beta}\int V_{\text{in}}(t)\mathrm{d}t - \frac{1}{\beta}\int i_{\text{BIAS}}(t)\mathrm{d}t. \tag{2.27}$$

All above expressions do not take into account nonlinear nature of piezoelectric ceramics that introduce large parts of uncertainty. For instance, measurements on a unimorph beam of $15\times1\times0.2\,\text{mm}$ showed $C_{\text{P}} = 1.74\,\text{nC/V}$ and $\beta = 1.03\,\text{nC/mN}$. Blocking force of such a beam was only 0.07 mN/V. This indicates that 1% of error (nonlinearity) in charge-to-applied voltage characteristic introduces 24% uncertainty in the estimation of force. Given that ferroelectric behaviour of the PZT material shows even 15% of nonlinearity, a compensation of these unwanted effects is unavoidable.

Hence, we will replace $\frac{-C_{\text{P}}}{C}V_{\text{in}}$ term from (2.26) with two models for hysteresis and creep. The Vout expression becoming:

$$V_{\text{out}} = (V_{\text{hyst}} + V_{\text{creep}}) + \frac{C_{\text{R}}}{C}V_{\text{in}} - \frac{\beta F_{\text{ext}}}{C} - \frac{1}{C}\int \frac{V_{\text{in}}(t)}{R_{\text{FP}}}\mathrm{d}t - \frac{1}{C}\int i_{\text{BIAS}}(t)\mathrm{d}t. \tag{2.28}$$

Final formula for estimated force will include two additional operators for nonlinear effects: $F_{\mathrm{C}}(s)$ for creep and $F_{\mathrm{H}}(s)$ for hysteresis compensation:

$$\hat{F}_{\mathrm{ext}} = -\frac{C}{\beta}V_{\mathrm{out}} + \frac{C_{\mathrm{R}}}{\beta}V_{\mathrm{in}} - \frac{1}{R_{\mathrm{FP}}\beta}\int V_{\mathrm{in}}(t)\mathrm{d}t - \frac{1}{\beta}\int i_{\mathrm{BIAS}}(t)\mathrm{d}t - \frac{1}{\beta}F_{\mathrm{C}}(s)\cdot V_{\mathrm{in}} - \frac{1}{\beta}F_{\mathrm{H}}(s)\cdot V_{\mathrm{in}}. \tag{2.29}$$

Formula for free ($F_{\mathrm{ext}} = 0$) piezoelectric beam displacement is taken from [9]:

$$\hat{\delta}_{\mathrm{free_s}} = -\frac{C}{\alpha}V_{\mathrm{out}} + \frac{C_{\mathrm{R}}}{\alpha}V_{\mathrm{in}} - \frac{1}{R_{\mathrm{FP}}\alpha}\int V_{\mathrm{in}}(t)\mathrm{d}t - \frac{1}{\alpha}\int i_{\mathrm{BIAS}}(t)\mathrm{d}t, \tag{2.30}$$

where α is the displacement coefficient.

When submitted to both external voltage and force, theoretical expression (2.23) is prone to nonlinearities, hence it is better to estimate the displacement with the following formula:

$$\hat{\delta}_s = \hat{\delta}_{\mathrm{free_s}} - \hat{F}_{\mathrm{ext}}/k_Z, \tag{2.31}$$

where k_Z is transverse mechanical stiffness of the beam.

The Simulink detection model of force and displacement implemented into a dSPACE real time controller sums several terms from expressions (2.29), (2.30) and (2.31) (see Fig. 2.21). As seen, a supplementary third-order low-pass Butterworth filter was introduced to cancel the noise of $\hat{F}_{\mathrm{ext}}/k_Z$ term from (2.21) which is far superior to $\hat{\delta}_{\mathrm{free_s}}$.

2.4.5 Self-Sensing Parameter Identification

Identification for displacement self-sensing method was already discussed in the Sect. 2.3. The parameters were bias current i_{BIAS}, leaking resistance R_{FP} and displacement coefficient α. For simplicity reasons, we suppressed dielectric absorption compensation (Q_{DA}) but that can be introduced from [9] if more accuracy is required. We will have to add a supplementary series of parameters intended for force self-sensing, such as: force sensitivity β, transverse stiffness k_Z, hysteresis operator F_{H}, and creep transfer function F_{C}.

Identification procedure may be done in the following possible manner.

2.4.5.1 Force Sensitivity β and Transverse Stiffness k_Z Identification or Estimation

Actuator is short-circuited (in fact $V_{\mathrm{in}} = 0$) and an external force step $F_{\mathrm{ext}} \neq 0$ is applied. In our case force was applied by slightly moving the force sensor

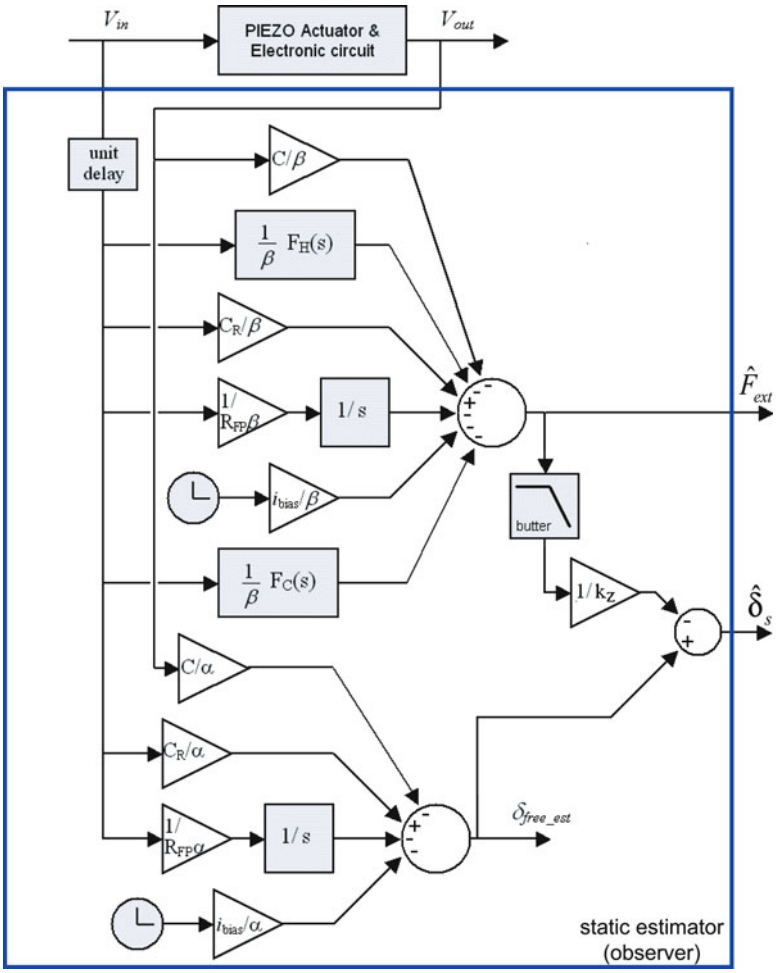


Fig. 2.21 Force and displacement detection observer implemented under Matlab Simulink. Reprinted with permission, Copyright 2009 American Institute of Physics [10]

(FT-S270) against the fixed actuator and therefore the applied force F_{ext} is known. Displacement, output voltage and force are recorded (Fig. 2.22). Force sensitivity β and beam stiffness k_Z are identified:

$$\begin{cases} k_Z = F_{\text{ext}}/(-\delta) \\ \beta = V_{\text{out}}/F_{\text{ext}}. \end{cases} \tag{2.32}$$

If a force sensor is not available, β parameter can be alternately calculated with only the laser displacement sensor aid. Transverse beam stiffness k_Z will

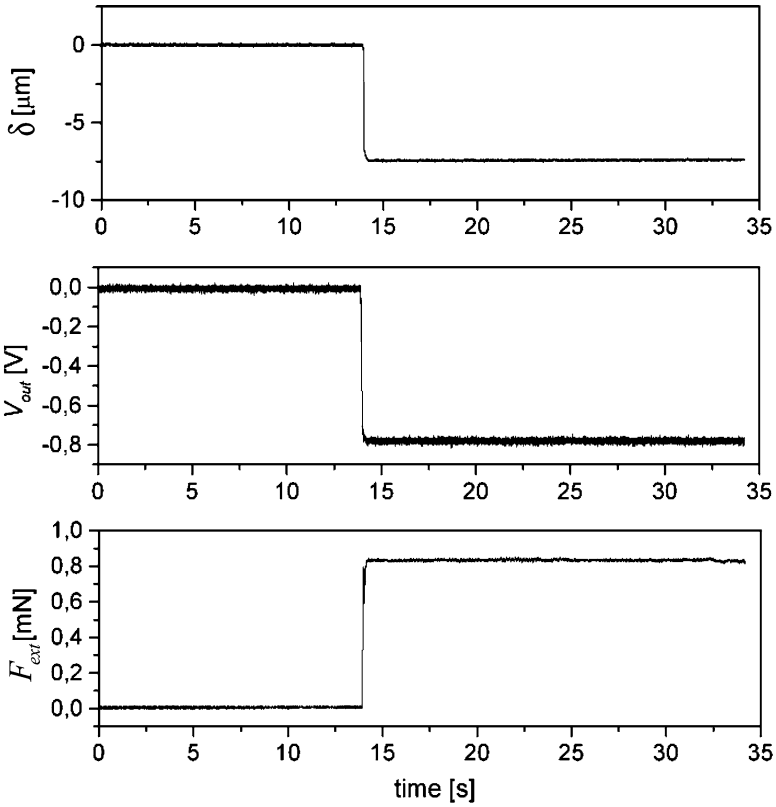


Fig. 2.22 Force sensitivity β and beam stiffness k_Z identification

be calculated based on known dimension and material properties. For a bi-morph cantilevered beam (Fig. 5), k_Z can be derived analytically from a known formula:

$$k_Z = 3YI/L^3 \tag{2.33}$$

where I is the bending moment of inertia around x_2.

Afterwards force sensitivity β will be estimated from:

$$\beta = V_{\text{out}}/(-\delta_{\text{meas}} k_Z). \tag{2.34}$$

2.4.5.2 Bias Current i_{BIAS} Identification

Bias current is known to vary exponentially with temperature. However, for a good amplifier and with some care regarding temperature variation, its influence will be small enough to consider i_{BIAS} constant [9]. Identification of i_{BIAS} is done under $F_{\text{ext}} = 0$, $V_{\text{in}} = 0$, $V_{\text{out}} \cong 0$ and stable environmental temperature, when current through the piezoelectric material is supposed null. The slight and linear V_{out} rate of change gives i_{BIAS} value, as in Fig. 2.23 (upper part).

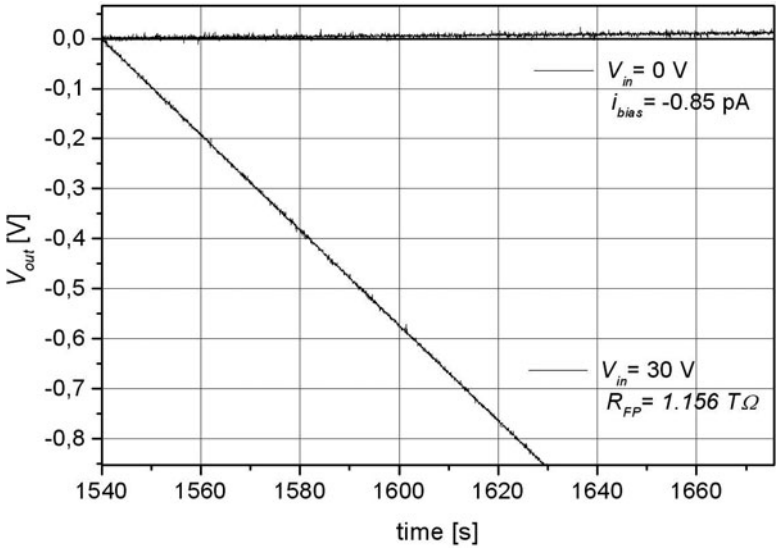


Fig. 2.23 Identification of bias and leakage current (resistance) of PZT actuator performed for input voltages of zero and +30 V, respectively

2.4.5.3 Leaking Resistance R_{FP} Identification

The procedure is similar to that presented in [9], under zero force $F_{\text{ext}} = 0$ and a constant applied voltage $V_{\text{in}} = 30\,\text{V}$ (see Fig. 2.23). After more than $1,000\,\text{s}$ the piezoelectric material relaxation (creep) becomes negligible and V_{out} rate of change only depends on bias current (already identified) and on leaking resistance to be identified from (2.26) or (2.27).

As seen from Fig. 2.23, for a good circuit the influence of leaking resistance at high values of V_{in} is more significant than that of bias current. For some applications i_{BIAS} can even be neglected.

2.4.5.4 Displacement Coefficient α Identification

A ramped step signal is applied to the actuator submitted to null external force ($F_{\text{ext}} = 0$). The ramped signal of around 20 V/s suppresses transition oscillations. Displacement δ, input and output voltages V_{in} and V_{out} are recorded, as in Fig. 2.24. Coefficient α that links output voltage to displacement is computed easily with values immediately after the voltage step (that occurs at 13 s in the Fig. 2.24).

In our case, identified displacement coefficient was $\alpha = 3.435 \times 10^{-3}\text{C/m}$.

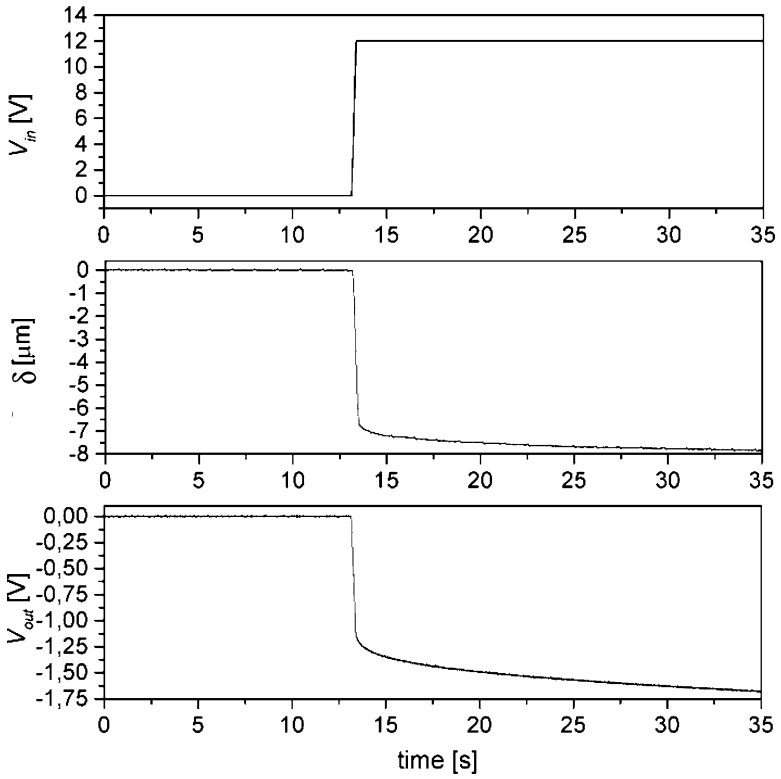


Fig. 2.24 Identification of α coefficient from a +12 V step input

2.4.5.5 Prandtl–Ishlinskii Hysteresis Operator Identification

It is well known that ferroelectric materials are characterized by hysteresis nonlinearity between applied voltage V_{in} and free actuator bending δ, as in Fig. 2.25.

There exist several hysteresis models for linearizing piezoelectric systems. The principle of the usually linearization method is the implemention of their inverse models (Fig. 2.26a), also known as feedforward compensation technique.

Cantilever bending δ is proportional with the charge [8,9]. In our case, there will be an inherent hysteresis between applied voltage V_{in} and output voltage V_{out}. Force self-sensing accuracy strongly depends on proper compensation of hysteresis. There are two equally possible options:

- Use of the feedforward compensation technique by cascading an inverse hysteresis operator, as in Fig. 2.26a
- Or substracting output signal with that of the direct operator (model). A principle scheme is given in Fig. 2.26b

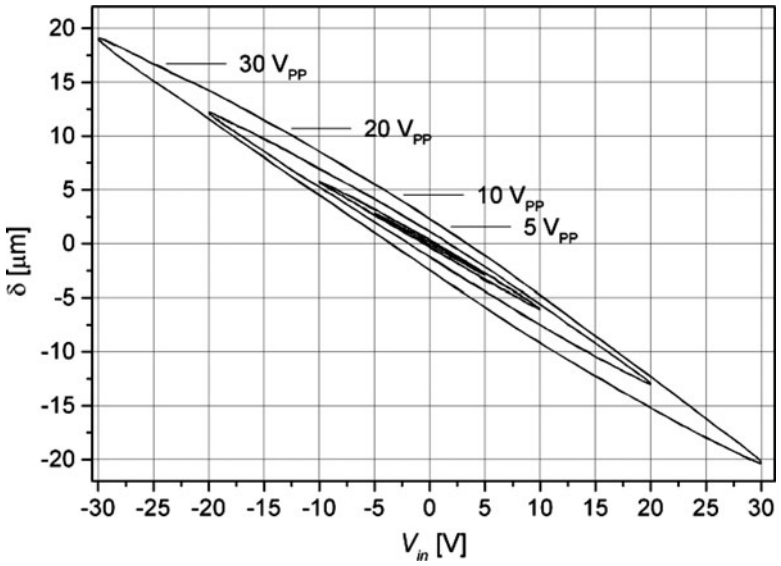


Fig. 2.25 Typical hysteretic behaviour of piezo actuators

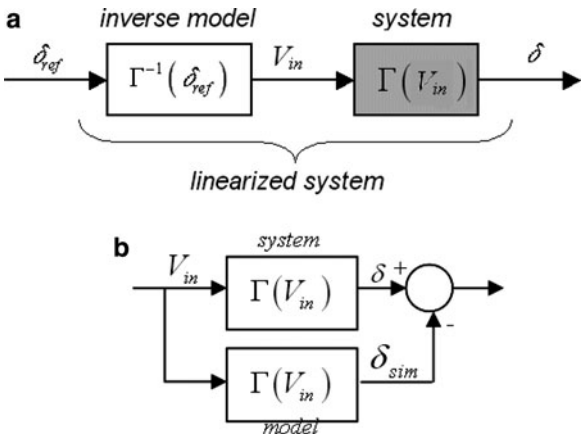


Fig. 2.26 (**a**) Nonlinear compensation of displacement by cascading the system with its inverse model. (**b**) Parallel compensation of nonlinear system. Reprinted with permission, Copyright 2009 American Institute of Physics [10]

The latter option (Fig. 2.26b) was chosen given the particularity that V_{in} applied signal can thus remains totally external to the self-sensing system (sometimes required by applications).

Hysteresis can be estimated/compensated with several methods: the Preisach model [30], the Prandtl–Ishlinskii model (PI) [3, 31, 32], the Bouc–Wen model [33] or asymmetric hyperbola shaped operator [34]. However, the PI model is especially appreciated for its ease of implementation, ease of obtaining the direct/inverse model and its accuracy. It was particularly discussed in previous papers [3].

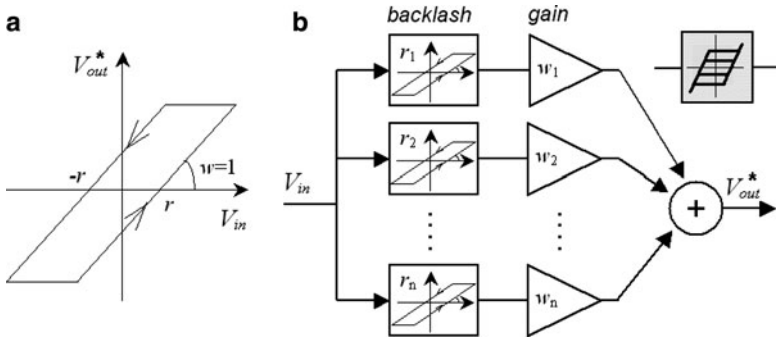


Fig. 2.27 (**a**) The play operator. (**b**) Prandtl–Ishlinskii (PI) hysteresis approximation

In the PI model, a hysteresis is based on the play operator, also called backlash operator. A play operator of unity slope, pictured in Fig. 2.27a, is defined by:

$$V^*_{\text{out}}(t) = \max\{V_{\text{in}}(t) - r, \min[V_{\text{in}}(t) + r, V^*_{\text{out}}(t - T)]\}, \tag{2.35}$$

where $V^*_{\text{out}}(t)$ is the output voltage compensated against bias and leaking currents, r is the radius of play operator and T is the sampling period.

A hysteresis can be approximated by the sum of several play operators weighted by the gain (slope) w_i [35]. Let n be the number of elements, so we have:

$$V^*_{\text{out}}(t) = F_{\text{H}}(V_{\text{in}}) = \sum_{i=1}^{n} w_i \cdot \max\{V_{\text{in}}(t) - r_i, \min[V_{\text{in}}(t) - r_i, V^*_{\text{out}}(t - T)]\}. \tag{2.36}$$

Figure 2.27b presents the implementation scheme in Simulink of the hysteresis PI model. If the number n is high, the model will be precise. However, it is too high, the model may become complex for implementation. Parameters $bw_i = 2r_i$ and w_i have been identified by using the steps presented in [3].

We developed a small program for PI hysteresis operator identification, as shown in [3]. Identification of w_i and r_i ($i = 1 \cdots n$) arrays is made with a couple triangular V_{in} signals of fixed slope and different amplitudes as in Fig. 2.28a, b. The slope should be low enough to avoid the phase-lag due to the dynamics of the cantilever, which therefore would modify the hysteresis curve. However, it should not be too low in order to avoid the influence of the creep on the same hysteresis curve. In our case the slope was chosen at ± 20 V/s. The maximum amplitude is chosen to be 30 V peak-to-peak, corresponding to the range use. The identification is performed with the signal of the largest amplitude. Smaller amplitude signals are further used for identified operator error evaluation. If errors are too high consider changing the signal slope or reduce the voltage interval.

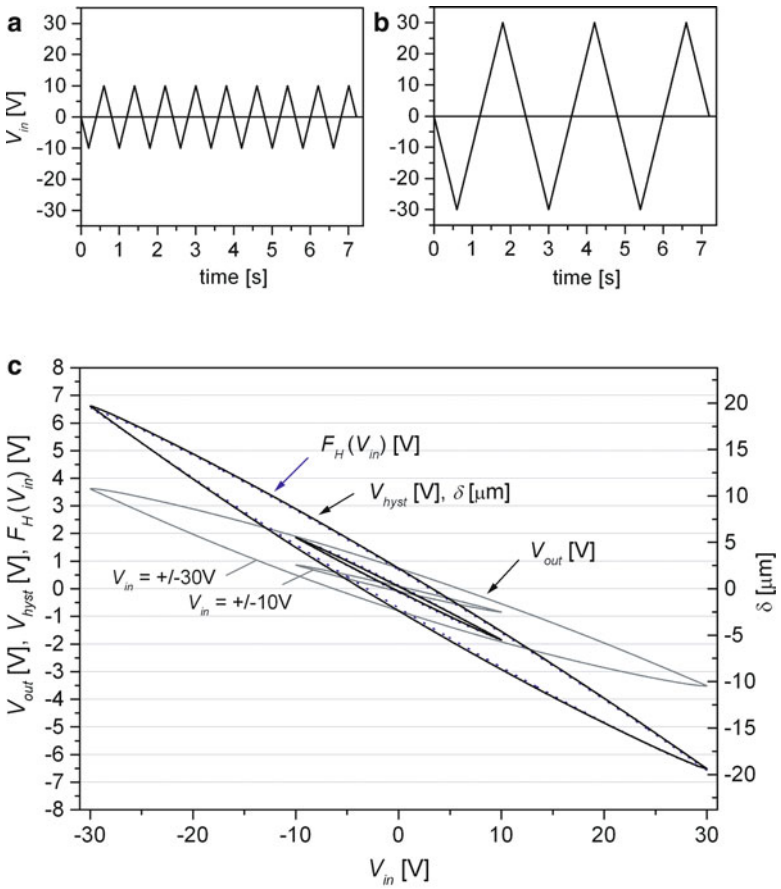


Fig. 2.28 (**a**)–(**b**) Applied Vin signals for hysteresis identification. (**c**) Experimental and identified curves

In Fig. 2.28c, experimental and identified hysteresis curves superpose in detail. Identified F_C operator consisted of $n = 40$ elements. For space-saving reasons, individual values are not represented; however, bw_i varied from 1.40 to 57.90 and w_i from -0.1179 to 0.2938.

2.4.5.6 Creep Transfer Function Identification

Creep effect is, like hysteresis, related to piezoelectric coefficients nonlinearity. Upon an applied V_{in} step signal, it is recorded that displacement will continue to drift for several hundred seconds (Fig. 2.29).

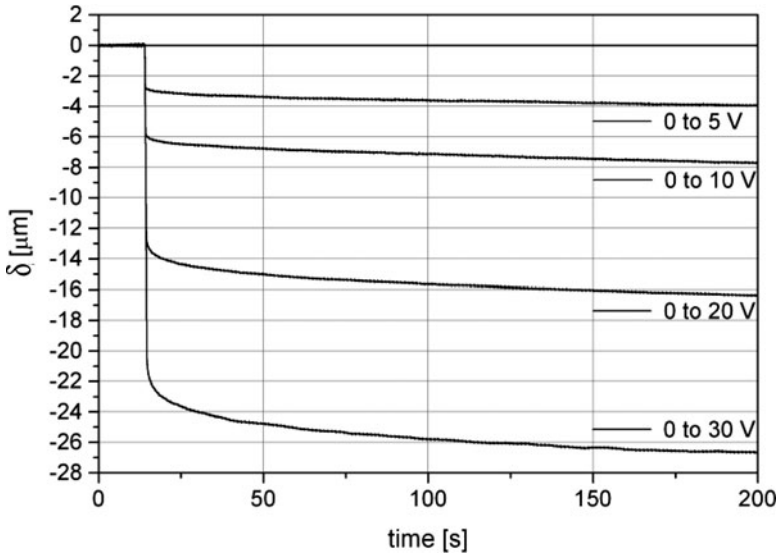


Fig. 2.29 Typical creep behaviour of a piezo actuator displacement for different voltage steps (ramped at 20 V/s)

The creep can be modeled with a linear time invariant (LTI) transfer function [3]. The identification of the creep operator $F_{CY}(V_{\text{in}})$ is performed as follows:

- A ramp input V_{in} is applied. The slope is the same to that used in hysteresis PI operator identification. In our case we used as $V_{\text{in}} = -10\,\text{V}$ as in Fig. 2.30a.
- The response is observed for a long duration of time (>200 s if possible) in order to well observe the creep.
- The creep part $V_{\text{creep}}(t)$ (Fig. 2.30b) is separated:

$$V_{\text{creep}} = \left(V_{\text{out}} - \frac{C_{\text{R}}}{C}V_{\text{in}} + \frac{1}{C}\int\left(\frac{V_{\text{in}}(t)}{R_{\text{FP}}} + i_{\text{BIAS}}\right)\text{d}t\right) - F_{\text{H}}(V_{\text{in}}). \tag{2.37}$$

- Having the input $V_{\text{in}}(t)$ and the output $V_{\text{creep}}(t)$, the model $F_{\text{C}}(V_{\text{in}})$ remains to be identified.

Several models with different orders were identified using the ARMAX method and Matlab. It seems that from the 3rd order, the error between the identified model and the experimental curve stops decreasing exponentially. We chose a model of 4rd order:

$$F_{\text{C}}(s) = \frac{V_{\text{creep}}(s)}{V_{\text{in}}(s)} = \frac{a_0 s^4 + a_1 s^3 + a_2 s^2 + a_3 s^1 + a_4}{s^4 + b_1 s^3 + b_2 s^2 + b_3 s^1 + b_4} \tag{2.38}$$

where $a_0 \ldots a_4$ and $b_1 \ldots b_4$ are numerator and denominator polynomial coefficients of creep transfer function.

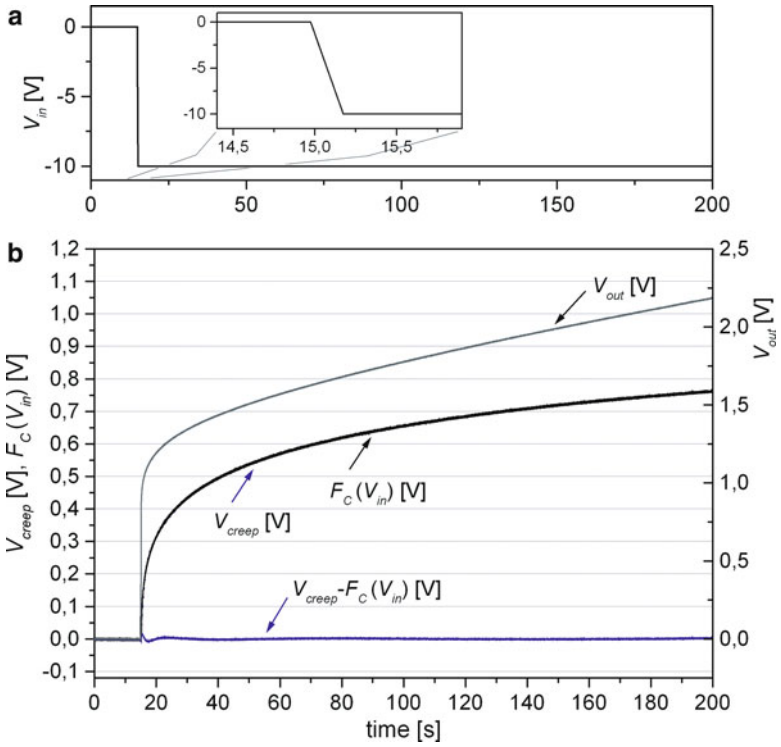


Fig. 2.30 (**a**) Applied signal for creep identification. (**b**) Experimental data and identified transfer function. Reprinted with permission, Copyright 2009 American Institute of Physics [10]

For instance, data plotted above were identified with the following transfer function:

$$F_C(s) = \frac{0.1601s^4 - 39.03s^3 - 767.1s^2 - 488.6s - 11.57}{s^4 + 130.3s^3 + 6.241e4s^2 + 1.229e4s + 145.5}. \tag{2.39}$$

2.4.6 Results and Discussion

In this section, some self-sensing results are presented issuing the explained schematic from Fig. 2.21 and subsequent identified parameters. A unimoph PZT on *Ni* cantilevered actuator ($15 \times 1 \times 0.28$ mm) is brought near the force sensor (close to contact) then a series of ramped negative periodic steps (Fig. 2.31) ranging from 0 to -10 and -20 V is applied, making the actuator to enter in contact and push the sensor. Maximum-recorded force was of 1.15 mN. As seen from Fig. 2.32, error between estimated and measured force sums 0.16 mN, meaning 14% (from $+8\%$ to -6%).

From Fig. 2.33 it results that total displacement is of 3 µm. Tip entered into contact with force sensor at 1.5 µm. Error between self-sensing method and optical sensor readings ranges from -0.65 to $+0.45$ µm (36% in total).

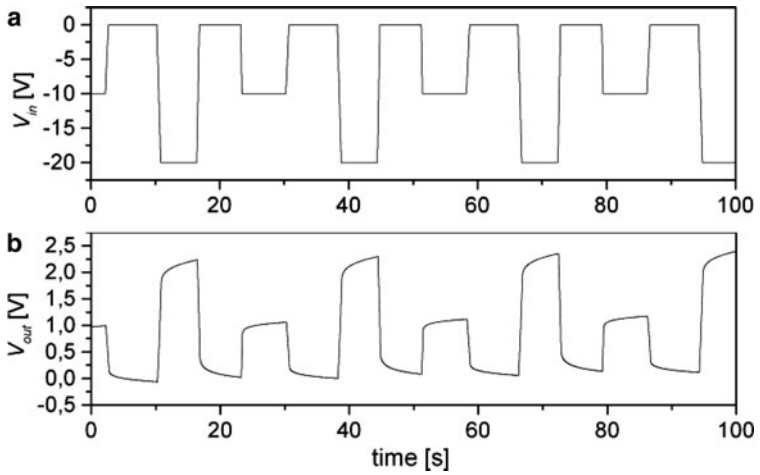


Fig. 2.31 (**a**) Arbitrary applied signal. (**b**) Corresponding output. Reprinted with permission, Copyright 2009 American Institute of Physics [10]

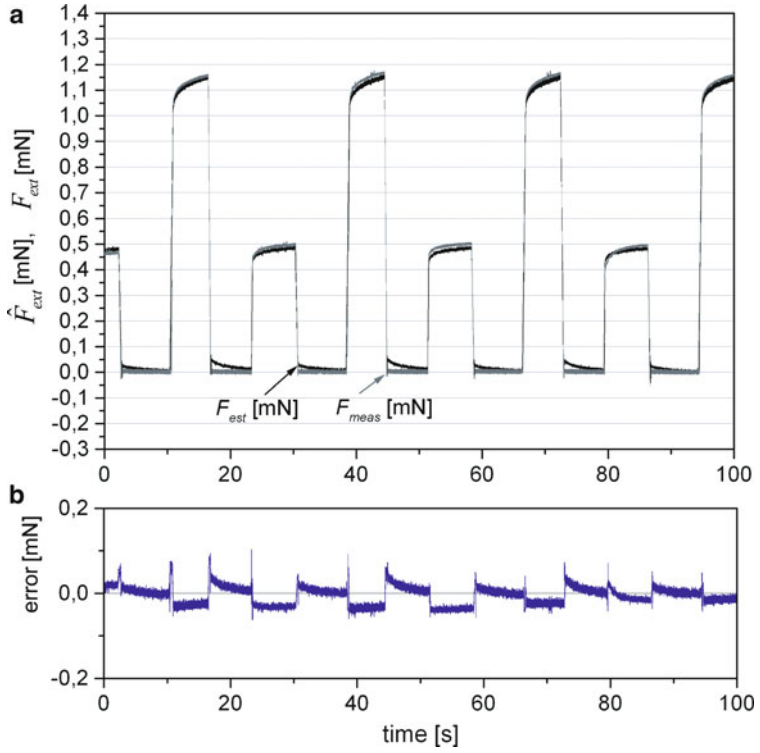


Fig. 2.32 (**a**) Measured and estimated force. (**b**) Absolute error. Reprinted with permission, Copyright 2009 American Institute of Physics [10]

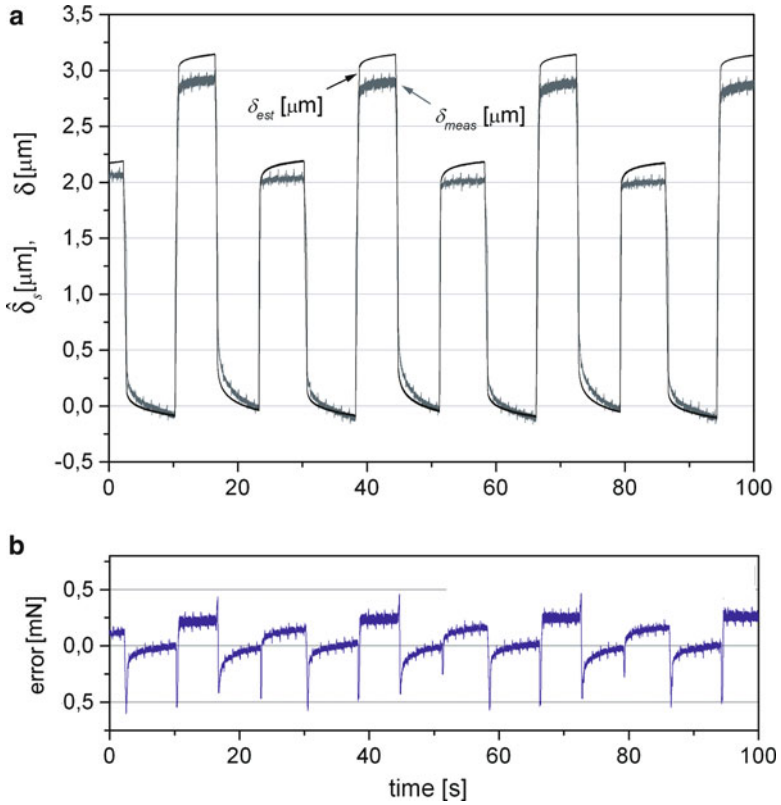


Fig. 2.33 (**a**) Measured and estimated tip displacement. (**b**) Absolute error

There are some limitations of the method. Displacement results are, as expected, slightly inferior in term of precision relative to those reported in only displacement self-sensing (see Sect. 2.3) but, in exchange, supplementary information about force was able to be provided. Also, as expected, force estimation is slightly less accurate in self-sensing actuator mode than in sensor-only mode (cantilever submitted only to external force) but the advantage of self-sensing consist in its double role. For instance self-sensing method would provide useful displacement and/or force information from the arms of a micro-gripper.

The displacement range or dynamics of the actuator are not influenced by the self sensing circuit, but as applied voltage increases, nonlinearties cause relative error to grow significantly, exceeding 50% for ± 40 V operation. To overcome that, more complex hysteresis operator compensation should be employed and extra close contact information would also help in ameliorating precision. Indeed, a very accurate hysteresis and creep modeling is required because 1% of error in charge estimation due to applied voltage may cause nearly 20–30% of error in force detection.

Dynamics were not taken into account as we tested the actuator in quasi-static at several Hz compared to the first resonant frequency at 630 Hz, faster tasks will require introduction of a dynamic term in Fig. 2.21 and expressions (2.29)–(2.31).

Ambient temperature fluctuation increase uncertainty especially for unimoph layered actuators; in our case measurements were performed at around 0.1°C stabilized temperature.

2.5 Dynamic Displacement Self-Sensing

2.5.1 Principle

In Sect. 2.3, we presented the self-sensing measurement of the displacement performed by a piezocantilever. The technique was afterwards extended to measure both the displacement and the force in Sect. 2.4. However, the validity of the two proposed schemes are only in the static aspect. Indeed for constant displacement and force, the estimates are equal to the real signals when $t \to \infty$:

$$\begin{cases} \hat{\delta}_s(t \to \infty) \cong \delta(t \to \infty) \\ \hat{F}_{\text{ext}}(t \to \infty) \cong F_{\text{ext}}(t \to \infty) \end{cases}. \tag{2.40}$$

Since they do not consider the dynamic aspect, they are not suitable for a control point of view. In this section, we extend the static displacement self-sensing in Sect. 2.3 into dynamic such that the measurement can be used in a feedback control application.

To extend the static displacement self-sensing into dynamic, we consider the initial scheme in Fig. 2.8 and add a dynamic part in the observer. We, therefore, obtain a dynamic estimator as depicted in Fig. 2.34 such that δ_{d} is the estimate displacement. The objective is to compute the gains of the dynamic part such that:

$$\hat{\delta}_{\text{d}}(t) \cong \delta(t);\ \forall t\,. \tag{2.41}$$

2.5.2 Computation of the Gains of the Dynamic Estimator

To compute the dynamic estimator, we first provide the transfer function between the static estimate $\hat{\delta}_s$ and the input voltage V_{in}. For that, denote $H(s)$ the transfer between V_{out} and V_{in}:

$$V_{\text{out}}(s) = H(s)V_{\text{in}}(s). \tag{2.42}$$

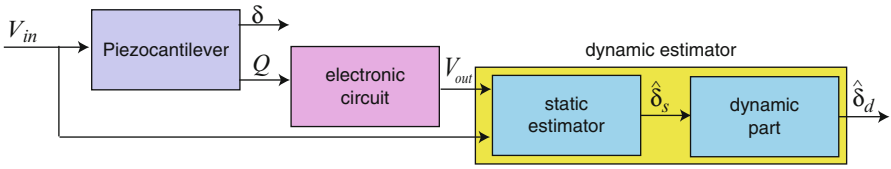
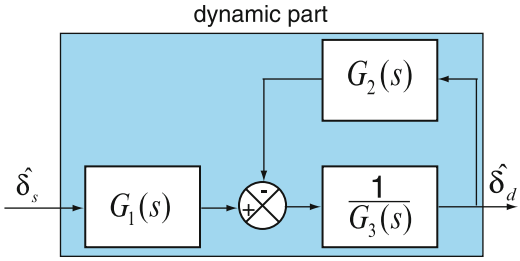


Fig. 2.34 Dynamic displacement self-sensing

Fig. 2.35 Block-scheme for the dynamic estimator



Applying the Laplace transformation to (2.8), and using (2.9) and (2.42), we derive the following transfer function:

$$\frac{\hat{\delta}_s}{V_{\text{in}}} = \left[c_1 H(s) + c_2 - \frac{c_3}{s} - \frac{k_s}{\tau s + 1} \right]. \tag{2.43}$$

Consider the structure in Fig. 2.35, called inverse multiplicative structure, as the block diagram of the dynamic part of the estimator [11]. In the structure, $G_1(s)$, $G_2(s)$ and G_3 are gains of the estimator to be computed. The main advantage of this scheme is that there is no direct inversion of transfer function which prevents us therefore from some conditions (bi-causality[1] and bi-stability) on the different models, except for $G_3(s)$ which is, as we will see, a non-null real number (and therefore invertible).

From Fig. 2.35, we have:

$$\frac{\hat{\delta}_d(s)}{\hat{\delta}_s(s)} = \frac{G_1(s)}{G_2(s) + G_3(s)}. \tag{2.44}$$

Employing (2.43) and (2.44), we obtain the full transfer function relating the estimate displacement $\hat{\delta}_{\text{d}}$ and the input control V_{in}:

$$\frac{\hat{\delta}_d(s)}{V_{\text{in}}(s)} = \left(\frac{G_1(s)}{G_2(s) + G_3(s)} \right) \left(c_1 H(s) + c_2 - \frac{c_3}{s} - \frac{k_s}{\tau s + 1} \right). \tag{2.45}$$

[1] Bi-causality means causality of the model and of its inverse.

Let us consider that the model relating the real displacement δ and the input control V_{in} of the piezocantilever is a LTI-model with a static gain K and a dynamic part $D(s)$, such that $D(s=0)=1$. So we have:

$$\frac{\delta(s)}{V_{\text{in}}(s)} = K \cdot D(s). \tag{2.46}$$

Thus, applying the condition (2.41)–(2.45) and (2.46) yields:

$$\left(\frac{G_1(s)}{G_2(s)+G_3(s)}\right) = \frac{K \cdot D(s)}{\left(c_1 H(s) + c_2 - \frac{c_3}{s} - \frac{k_s}{\tau s+1}\right)} \tag{2.47}$$

which permits us to define the gains of the dynamic part of the estimator as follows:

$$\begin{cases} G_1(s) = K \cdot D(s) \\ G_2(s) = c_1 H(s) - \dfrac{c_3}{s} - \dfrac{k_s^*}{\tau s+1}. \\ G_3(s) = c_2 \end{cases} \tag{2.48}$$

From this result, it is confirmed that there is indeed no inversion of the transfer functions $D(s)$ and $H(s)$ as expected.

2.5.3 Parameters Identification

The experimental setup already used before is used here. Thus, the different parameters related to the static self-sensing are known and only K, $D(s)$ and $H(s)$ have to be identified. For that, we apply a step voltage $V_{\text{in}} = 20\,\text{V}$ to the cantilever. The output deflection δ of the cantilever is captured using the optical sensor. It allows the identification of K and $D(s)$ accordingly to (2.46). At the same time, the output voltage V_{out} is also captured which, according to (2.42), allows us identify $H(s)$. Figure 2.36 pictures the experimental results.

Applying the ARMAX systems identification to these experimental results, we obtain:

$$\begin{cases} K = 0.69 \left[\dfrac{\mu\text{m}}{\text{V}}\right] \\ D(s) = \dfrac{5.752 \times 10^{-3}(s+3.062\times10^4)(s^2-1.95\times10^4 s+3.076\times10^8)}{(s+3976)(s^2+54.37s+1.362\times10^7)} \end{cases} \tag{2.49}$$

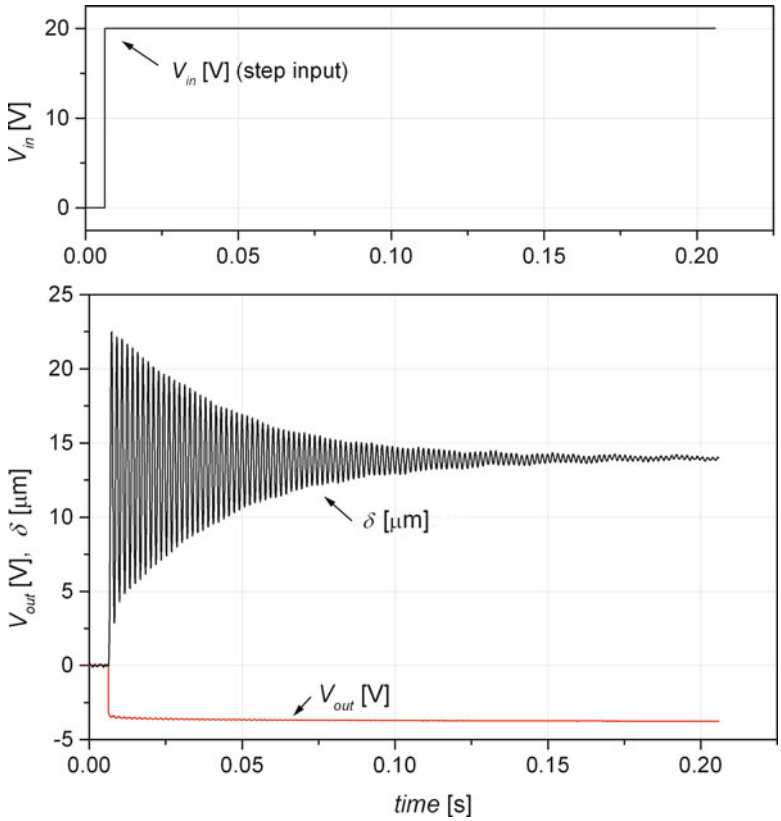


Fig. 2.36 Step response on the deflection δ and on the output voltage V_{out}

and

$$H(s) = \frac{-0.1584(s+5.911\times10^4)(s+236)(s+13.74)}{(s+5.541\times10^4)(s+224)(s+12.99)}. \tag{2.50}$$

2.5.4 Dynamic Displacement Self-Sensing Experimental Results

In order to prove the efficiency of the dynamic displacement self-sensing, it is implemented and the result is compared with that of the static displacement self-sensing. For that, a step input voltage $V_{\text{in}} = 20\,\text{V}$ is applied to the piezocantilever. The estimate $\hat{\delta}_{\text{s}}$ corresponding to the static self-sensing is captured. We also captured the estimate $\hat{\delta}_{\text{d}}$ of the dynamic self-sensing. Figure 2.37 shows the results. They clearly show that the measurement $\hat{\delta}_{\text{d}}$ from the dynamic self-sensing well captures both the transient part and the final value of the deflection δ while $\hat{\delta}_{\text{s}}$ from the static self-sensing only captures the final value.

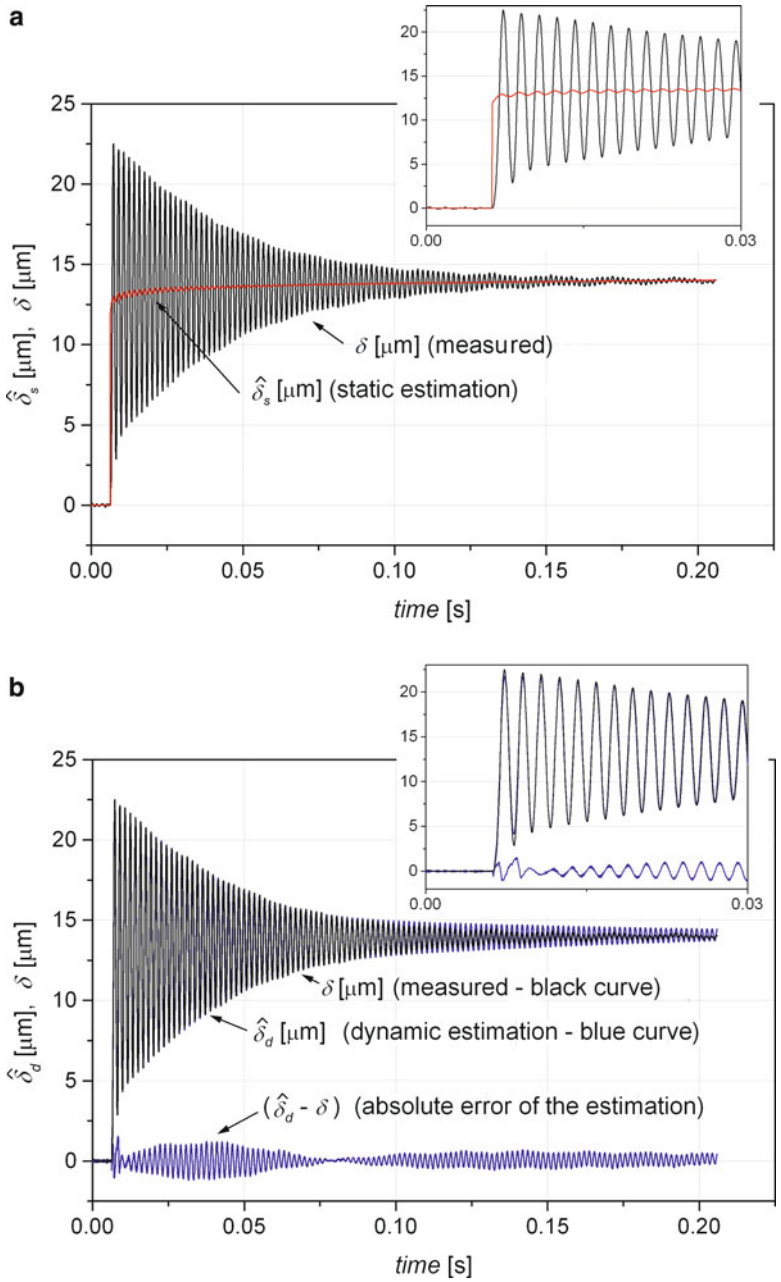


Fig. 2.37 (**a**) Result with the static displacement self-sensing. (**b**) Result with the dynamic displacement self-sensing

2.6 Conclusion

This chapter documented a self-sensing method to observe either displacement-only or both displacement/force observation at the tip of cantilevered piezoelectric actuators, generally when the latter is in contact with objects. Both the static and dynamic aspectes are accounted. The nonlinearities of piezoelectric coefficients causing static hysteresis and creep unwanted behaviour were taken into account and compensated allowing improving the proposed techniques in term of the precision. While the static hysteresis was identified with a Prandtl-Ishlinskii model, the creep was approximated by a 4th order LTI transfer function whose parameters were identified using ARMAX method. Furthermore, leakage resistance was also compensated. The proposed method is convenient for quasi-static applications as well as for feedback control utilization, such as in micromanipulation/microassembly tasks where several seconds of periods and control context are required.

References

1. Micky Rakotondrabe, Cédric Clévy and Philippe Lutz, "Modelling and robust position/force control of a piezoelectric microgripper", IEEE International Conference on Automation Science and Engineering (CASE), pp. 39–44, Scottsdale AZ USA, Sept 2007.
2. Micky Rakotondrabe and Alexandru Ivan, "Development and force/position control of a new hybrid thermo-piezoelectric microGripper dedicated to micromanipulation tasks", IEEE - Transactions on Automation Science and Engineering (T-ASE), DOI.10.1109/TASE.2011.2157683, 2011.
3. M. Rakotondrabe, C. Cléy and P. Lutz, "Complete open loop control of hysteretic, creeped and oscillating piezoelectric cantilevers", IEEE Transactions on Automation Science and Engineering (TASE), Vol.7(3), pp. 440–450, July 2010.
4. Jeffrey J. Dosch, Daniel J. Inman and Ephrahim Garcia, "A self-sensing piezoelectric actuator for collocated control", Journal of Intelligent Material Systems and Structures, Vol.3(1), pp. 166–185, January 1992.
5. W.W. Law, W-H. Liao and J. Huang, "Vibration control of structures with self-sensing piezoelectric actuators incorporating adaptive mechanisms", Smart Materials and Structures, Vol. 12, pp. 720–730, 2003.
6. Chee Khiang Pang, Guoxiao Guo, B. M. Chen, Tong Heng Lee "Self-sensing actuation for nanopositioning and active-mode damping in dual-stage HDDs", IEEE/ASME Transactions on Mechatronics (T-mech), Vol.11(3), pp. 328–338, 2006.
7. S. O. R. Moheimani and Y. K. Yong, "Simultaneous sensing and actuation with a piezoelectric tube scanner", Review of Scintific Instruments, 79, 073702, 2008
8. S. O. R. Moheimani, "Invited Review Article: Accurate and fast nanopositioning with piezoelectric tube scanners: Emerging trends and future challenges", RReview of Scintific Instruments, 79, 071101, 2008.
9. Alexandru Ivan, Micky Rakotondrabe, Philippe Lutz and Nicolas Chaillet, "Quasi-static displacement self-sensing method for cantilevered piezoelectric actuators", Review of Scientific Instruments (RSI), Vol.80(6), 065102, June 2009.
10. Alexandru Ivan, Micky Rakotondrabe, Philippe Lutz and Nicolas Chaillet, "Current integration force and displacement self-sensing method for cantilevered piezoelectric actuators", Review of Scientific Instruments (RSI), Vol.80(12), 2126103, December 2009.

11. Micky Rakotondrabe, Ioan Alexandru Ivan, Sofiane Khadraoui, Cédric Clévy, Philippe Lutz and Nicolas Chaillet, “Dynamic displacement self-sensing and robust control of cantilevered piezoelectric actuators dedicated to microassembly tasks”, IEEE/ASME - AIM, (International Conference on Intelligent Materials) 2010, pp:557–562, Montreal Canada, July 2010.
12. J.G. Smits and S.I. Dalke, “The constituent equations of piezoelectric bimorphs”, IEEE Ultras. Symp. pp. 781–784, 1989.
13. S. Muensit et al., “Piezoelectric coefficients of multilayer Pb(Zr,Ti)O3 thin films”, Appl. Phys. A, 92, pp. 659–663, 2008.
14. T.S. Low and W. Guo, “Modelling of a three-layer piezoelectric bimorph beam with hysteresis”, J. Microelectro mech. Syst., vol. 4, no. 4, pp. 230–236, 1995.
15. H. J. M. T. A. Adriaens, W. L. de Koning, and R. Banning, “Modelling piezoelectric actuators”, IEEE/ASME Trans. on Mechatronics, vol. 5, no. 4, pp. 331–341. 104–110, 2008.
16. Y-G. Zhou et al., “Modeling of sensor function for piezoelectric bender elements”, J. Zhejiang Univ. Sci. A. 9(1), 1–7, 2008.
17. R. J. Wood, E. Steltz, and R. S. Fearing, “Nonlinear performance limits for high energy density piezoelectric bending actuators”, Proc. to IEEE ICRA, Spain, 2005.
18. Takigami et al., “Application of self-sensing actuator to control of a soft-handling gripper”, Proc. to IEEE ICCA, pp. 902–906, Italy, 1998.
19. H. Jung, J.Y. Shim and D. Gweon, “New open-loop actuating method of piezoelectric actuators for removing hysteresis and creep” Review of Scientific Instruments, 71 (9), pp. 3436–3440, 2000.
20. K. Kuhnen, H. Janocha, “Compensation of the creep and hysteresis effects of piezoelectric actuators with inverse systems”, Actuator 98, Proceedings 6th International Conference on New Actuators (Bremen 17.-19.6.1998), Bremen: ASCO-Druck, pp. 426–429, 1998.
21. R. Changhai and S. Lining, “Hysteresis and creep compensation for piezoelectric actuator in open-loop operation”, Sensors and Actuators, 2005, vol. 122, no1, pp. 124–130.
22. J. Minase, T-F. Lu and B.Cazzolato, “Adaptive identification of hysteresis and creep in piezoelectric stack actuators”, Proc. to 8th Int. Symp. for Meas. Tech. and Intell. Instr. (ISMTII), Japan, 2007.
23. Y. Cui et al. “Self-sensing compounding control of piezoceramic micro-motion worktable based on integrator”, Proc. to 6th World Cong. On Intell. Con. and Autom., China, 2006.
24. A. Badel et al. “Self sensing force control of a piezoelectric actuator”, IEEE Trans. on UFFC, vol. 55, no. 12 pp. 2571–2581, 2008.
25. A. Badel et al., “Self-sensing high speed controller for piezoelectric actuator”, J. of Intell. Mater. Syst. and Struct., vol 19, no. 3, pp. 395–405, 2008.
26. M. Goldfarb and N. Celanovic, “Modeling piezoelectric stack actuators for control of micromanipulation”, IEEE Control Systems Magazine, vol. 3, no. 3, pp. 69–79, 1997.
27. A. S. Putra et al., “With Adaptive Control in Applications With Switching Trajectory”, IEEE/ASME Trans. on Mechatronics, vol. 13, no. 1, pp. 104–110, 2008.
28. D. Campolo, R. Sahai, R.S. Fearing, “Development of piezoelectric bending actuators with embedded piezoelectric sensors for microelectromechanical flapping mechanisms”, Proc. to IEEE Int. Conf. on Robot. Autom. Vol. 3, pp. 3339–3346, Taipei, 2003.
29. J. G. Smits and W-S. Choi., “The constituent equations of piezoelectric heterogeneous bimorphs”, IEEE Ultrasonic Symposium, pp. 1275–1278, 1990.
30. A. Dubra and J. Massa and C.l Paterson, “Preisach classical and nonlinear modeling of hysteresis in piezoceramic deformable mirrors”, Optics Express, pp. 9062–9070, 2005.
31. K. Kuhnen and H. Janocha, “Inverse feedforwrad controller forcomplex hysteretic nonlinearities in smart-materials systems”. Control and Intelligent Systems, vol. 29, no. 3, pp. 74–83, 2001.
32. B. Mokaberi and A. A. G. Requicha, “Compensation of scanner creep and hysteresis for AFM nanomanipulation”, IEEE Trans. on Autom. Sci. and Eng., pp. 197–208, 2008.
33. Micky Rakotondrabe, “Bouc-Wen modeling and inverse multiplicative structure to compensate hysteresis nonlinearity in piezoelectric actuators”, IEEE - Transactions on Automation Science and Engineering (T-ASE), Vol.7, Issue.4, DOI.10.1109/TASE.2010.2081979, December 2010.

34. A. Badel, J. Qiu and T. Nakano, “A New Simple Asymmetric Hysteresis Operator and its Application to Inverse Control of Piezoelectric Actuators”, IEEE Trans. on UFFC, Vol. 55–5, pp. 1086–1094, 2008.
35. M.A. Krasnosel’skii and A.V.Pokrovskii, “Systems with Hysteresis”, Springer-Verlag, Berlin, New York, 1989 (410p).



http://www.springer.com/978-1-4419-9945-0

Signal Measurement and Estimation Techniques for Micro and Nanotechnology

Clévy, C.; Rakotondrabe, M.; Chaillet, N. (Eds.)

2011, X, 242 p., Hardcover
ISBN: 978-1-4419-9945-0